A STUDY IN CULTURED NEURONAL NETWORKS

by

Fazlı Kemal Bayat

B.S., in Electrical Engineering, Yıldız Technical University, 2006

M.S., in Electrical Engineering, Yıldız Technical University, 2009

Submitted to the Institute of Biomedical Engineering

in partial fulfillment of the requirements

for the degree of

Doctor

of

Philosophy

Boğaziçi University

2021

A STUDY IN CULTURED NEURONAL NETWORKS

APPROVED BY:

Prof. Dr. Albert Güveniş .....
(Thesis Advisor)

Prof. Dr. Halil Özcan Gülçür .....
(Thesis Co-advisor)

Prof. Dr. Gürkan Öztürk .....

Assoc. Prof. Dr. Bora Garipcan .....

Prof. Dr. Ahmet Ademoğlu .....

Prof. Dr. Ramazan Bal .....

DATE OF APPROVAL: 13 July 2021

ACKNOWLEDGMENTS

I acknowledge the Boğaziçi University Research Fund, for the support to our study under the Project Code 8080D. I am grateful to the Regenerative and Restorative Medicine Center (REMER) of Istanbul Medipol University for their generous permission to use facilities and supplies.

I am extremely thankful to my supervisors Prof. Dr. Halil Özcan Gülçür and Prof. Dr. Albert Güveniş, for their noble patience, guidance, and support. I owe an enormous of gratitude to Prof. Dr. Gürkan Öztürk, who believed in our study and provided support and guidance through each stage. I would like to express my appreciation to my committee member, Assoc. Prof. Dr. Bora Garipcan for his constructive contributions and suggestions throughout this study. I would also like to thank my interviewees, Prof. Dr. Ahmet Ademoğlu and Prof. Dr. Ramazan Bal, who so graciously took time out of their busy schedules and provided detailed feedback and extensive comments.

ACADEMIC ETHICS AND INTEGRITY STATEMENT

I, Fazlı Kemal Bayat, hereby certify that I am aware of the Academic Ethics and Integrity Policy issued by the Council of Higher Education (YÖK) and I fully acknowledge all the consequences due to its violation by plagiarism or any other way.

Name :

Signature:

Date:

ABSTRACT

A STUDY IN CULTURED NEURONAL NETWORKS

In this study, two platforms, combining multi-electrode arrays and optogenetic methods, were developed to study living neural networks in vitro. Both platforms, which included stimulation of neural networks developed in culture and monitoring of their activities, were tested using primary neuronal cultures obtained from mice and their operability and usability were demonstrated. In the first platform, dorsal root ganglion cells were made to emit fluorescent light when calcium influx occurs by optogenetic technique. In this platform stimulation was provided electrically through multiple electrode arrays and experiments were performed under fluorescent microscopy. The evoked activity was monitored through calcium transitions and the analyzed results revealed the network connections. Next, the network connections determined by analysis were confirmed by immunostaining that showed connections physically. The results obtained illustrated that the dorsal root ganglion nerve cells could establish connections with each other to form networks. In the second platform, hippocampal cells were used and neurons were made excitable with light using the optogenetic approach. After that, the optical stimulation using a digital micro mirror device for excitation was performed locally and focused. Spontaneous and stimulated extracellular electrical activity was monitored and recorded with multiple electrode arrays. On this platform, bilateral and closed-loop electrophysiology applications were performed and multi-channel and experiment examples were presented. The results show that the new platform designed for extracellular electrophysiology applications, with the option of multi-channel, artifact-free and closed-loop experimentation, eliminates the deficiencies and problems of those proposed in the previous studies. In conclusion, in the presented study, it has been shown that multi-electrode arrays can be successfully integrated with optogenetic methods that have both activity monitoring and stimulation purposes.

Keywords: Cultured Neuronal Network, Multi Electrode Array, Optogenetics.

ÖZET

EKİLİ SİNİRSEL AĞLARIN İNCELENMESİ

Bu çalışmada canlı sinir ağlarını in vitro incelemek üzere çoklu elektrot dizileri ve optogenetik yöntemlerin bir araya getirildiği iki platform geliştirildi. Kültürde gelişen sinirsel ağların uyarımını ve etkinliklerinin izlenmesini içeren her iki platform, fareden elde edilen primer sinir kültürleri kullanılarak test edilerek işlerlik ve kullanılabilirlikleri gösterildi. İlk platformda arka kök gangliyon sinir hücreleri optogenetik yöntem ile kalsiyum giriş çıkışlarında floresan ışıma yapar hale getirildi. Floresan mikroskobi altında gerçekleştirilen bu platformda uyarım ise elektriksel olarak çoklu elektrot dizileri üzerinden sağlandı. Uyarılmış etkinlik kalsiyum geçişleri üzerinden izlendi ve elde edilen sonuçlar çözümlenerek ağ bağlantıları ortaya kondu. Ardından, çözümleme ile ortaya konulan ağ bağlantıları hücre boyaması uygulanarak fiziksel olarak da gösterilerek doğrulandı. Elde edilen sonuçlar arka kök gangliyon sinir hücrelerinin birbirleri ile bağlantı oluşturup ağ kurabildiklerini ortaya koymuş oldu. İkinci platformda ise hipokampal hücreler kullanıldı ve sinir hücreleri optogenetik yöntem kullanılarak ışık ile uyarılabilir hale getirildi. Bunun ardından, uyarım için bir sayısal mikro ayna aygıtından yararlanılarak kullanılan optik yöntem yerel ve odaklı olarak gerçekleştirildi. Kendiliğinden ve uyarılmış hücre dışı elektriksel etkinlik çoklu elektrot dizileri ile izlenerek kayıt altına alındı. Bu platformda çift taraflı ve kapalı çevrim elektrofizyoloji uygulamaları çok kanallı olarak gerçekleştirilerek deney örnekleri sunuldu. Elde edilen sonuçlar hücre dışı elektrofizyoloji uygulamaları için çok kanallı, artefaktsız ve kapalı çevrim deney yapma seçeneği ile önceki çalışmalarda bulunan eksikliklerin ve sorunların giderildiği yeni bir platform oluşturulduğunu gösterdi. Sonuç olarak, ortaya konulan çalışmada, çoklu elektrot dizilerinin hem etkinlik izleme hem de uyarım vermede kullanılan optogenetik yöntemlerin başarı ile entegre edilebildiği gösterilmiştir.

Anahtar Sözcükler: Ekili Sinirsel Ağ, Çoklu Elektrot Dizisi, Optogenetik.

TABLE OF CONTENTS

ACKNOWLEDGMENTS iii
ACADEMIC ETHICS AND INTEGRITY STATEMENT iv
ABSTRACT v
ÖZET vi
LIST OF FIGURES ix
LIST OF TABLES xiv
LIST OF SYMBOLS xv
LIST OF ABBREVIATIONS xvi
1. INTRODUCTION 1
1.1 Background 1
1.1.1 Cultured Neuronal Networks 1
1.1.2 Multi and Micro Electrode Arrays 2
1.1.3 Optogenetics 4
1.1.4 Integration of MEAs and Optogenetic Tools 5
1.2 Outline 6
2. PLATFORM I: ADULT MOUSE DORSAL ROOT GANGLIA NEURONS FORM ABERRANT GLUTAMATERGIC CONNECTIONS IN DISSOCIATED CULTURES 8
2.1 Introduction 9
2.2 Methods 11
2.2.1 Ethics statement and animal handling 11
2.2.2 Dissociated DRG culture protocol 11
2.2.3 Immunocytochemistry 12
2.2.4 Preparation of MEAs 12
2.2.5 Local electrical stimulation 14
2.2.6 Experimental procedure 15
2.2.7 Image analysis and statistics 16
2.3 Results 17

2.3.1 Stimulated neuronal responses activate other neurons via glutamatergic connections . . . 21
2.3.2 Higher order synaptic interactions . . . 23
2.3.3 Structural verification of synapses . . . 24
2.4 Discussion . . . 24
3. PLATFORM II: A NOVEL TOOL FOR CLOSED LOOP EXTRACELLULAR ELECTROPHYSIOLOGY - IMPLICATIONS FOR CULTURED NEURONAL NETWORKS . . . 29
3.1 Introduction . . . 30
3.2 Materials and Methods . . . 32
3.2.1 MEAs . . . 32
3.2.2 Culture Protocol . . . 33
3.2.3 Optogenetics . . . 35
3.2.4 Electrical Recording . . . 35
3.2.5 Software . . . 36
3.2.6 DLP Stimulation Setup . . . 37
3.3 Results . . . 38
3.3.1 Light Intensity . . . 39
3.3.2 Frequency and Duty Cycle . . . 40
3.3.3 Experimental Procedures . . . 41
3.3.4 Closing the Loop . . . 41
3.4 Discussion . . . 44
3.4.1 Implications for Cultured Neuronal Networks . . . 47
3.4.2 Concluding Remarks . . . 48
4. CONCLUSION . . . 49
APPENDIX A. Solutions and Media . . . 51
APPENDIX B. List of publications produced from the thesis . . . 53
REFERENCES . . . 54

LIST OF FIGURES

Figure 2.1 **a: A typical stimulation strategy.** A stimulation consists of two biphasic pulses of 400 μs duration, repeated in 0.5 s. Stimulation is repeated within six second periods. **b: Schematic representation of the experimental procedure.** Timelapse imaging and electrical stimulation of GCaMP6s expressing neurons using a MEA headstage placed on an inverted fluorescent microscope. Acquisition of calcium responses and live monitoring. Offline event detection, analysis and rendering of analog voltage signals. 13

Figure 2.2 Phase contrast (a1) and fluorescent (a2) images of typical cultures of DRG neurons. The cultures were grown on MEA plates with an average density of 100 cells/mm2. Fluorescent image shows the GCaMP6s expression of transgenic glutamatergic neurons at DIV3. Scale bar: 50 μm at 10x magnification. The illustration of ε- and complementary neighborhood definitions (b). 14

Figure 2.3 **Experimental steps.** Step one: Spontaneous activity recording prior to stimulation. Step two: electrical stimulation applied. Step three: Stimulation repeated after cultures were treated with blockers for 1h. Step four: Stimulation repeated after washout and 1h incubation. Yellow and black traces show activities of the same c^+ and c^- primary neuron at each step respectively. Blue shaded areas show subthreshold. Red dashes show stimulation instants. Each stimulation trace corresponds to a 2 Hz dual-biphasic pulses repeated in 6 sec periods. Vertical axis shows normalized $\Delta F/F(t)$. 18

Figure 2.4 **Response profiles of c^+ and c^- neurons.** Individual experiments are shown in color and the averaged response is shown in black. The first row shows the responses of c^- neurons and the second row shows the responses of c^+ neurons. The left and right column shows responses to stimulation in default and blocked cases, respectively. Red dashed lines show stimulation instants. Stimulation period is six seconds. Vertical axis shows normalized $\Delta F/F(t)$. 19

Figure 2.5 **Basic interactions.** (a) is an example for a c^- primary neuron and (b) and (c) are for c^+ primary neurons. Secondary neurons in (b) and (c) represent previously silent and previously spontaneously active types respectively. Fluorescent images show the locations of the stimulation electrode and the neuron bodies in a1, b1, and c1 (Scale bar: 50 μm, magnification: 10×). Stimulation instants and the corresponding time-series of calcium activity recorded in absence (left) and presence (right) of glutamatergic antagonists, a2, b2, c2. 20

Figure 2.6 **Multi-layered interactions.** Time-series of ROIs 1-9, ROI 1 is a c- primary neuron and ROIs 2-9 are secondary neurons (a). The stimulation voltage applied in three steps (2V-3V-2V) indicated as (i, ii, iii). (b) shows the averaged responses to individual stimuli detected in three voltage steps (n = 10 for (i) and (iii) steps, n = 20 for (ii) part). Response amplitude alterations are shown in normalized averaged values (c). Response amplitudes of ROIs 1, 4, 5 and 9 increased significantly from step (i) to (iii) ($p<0.05$). Hierarchical groups are shown, based on significant correlations ($p<0.05$) (d) and the connectivity strength values calculated with significant MPC scores ($p<0.05$), (e) obtained from connectivity analyses. 22

Figure 2.7 **Immunocytochemistry.** DRG culture on a MEA plate fixed on DIV3. Top: Figure shows maximum intensity projection of 14 z-stack images acquired in various depths, merging 3 channels. β-III Tubulin is shown in red, Synaptophysin is shown in green and DAPI is shown in blue. Bottom: (1) and (2) show a soma-axon connection and an axon terminal in detail. The axon-axon intersection sites are observed widespread. The a, b, c and d labels showtubulin, synaptophysin, DAPI and brightfield channels. Objective: 40×, scale bar:10 μm. 25

Figure 3.1 Capital letters represent some of the crucial components or procedures of the experimental platform II. (A) Opsin Transfection: Transduction of neurons with adeno-associated virus-mediated lightsensitive channel proteins. (B) MEA Recording: Extracellular action potentials being recorded from hippocampal cells cultured on Multi Electrode Array plates. (C) Microscopic Imaging: Observation of applied stimulation patterns with an inverted microscope. (D) Monitoring Data: Neuronal activity through 64 channels of the MEAs coupled to the data acquisition system. (E) Stimulation Pattern: Closing of the loop by application of designed stimulation patterns with the digital light processing projection system. 30

Figure 3.2 **CNNs on MEA plates.** (a) A 5×5cm MEA plate. (b) Location of the cells on the electrode surface DIV18. (c) and (d) Layout and scale features of MMEP-4 and MMEP-4R plates. Distances between electrodes are 150 and 70 μm for c and d. (e) and (f) Light spots circling the electrodes for calibration. 70 and 40 μm are averaging diameters of the light spots for e and f. Light spots were refracted through 1 mm thick glass and culture media. 34

Figure 3.3 **Flow diagram.** Dashed rectangle at left and right portions of the diagram indicate wetware and software parts, since the blocks on upper and lower sections show interface units. (1), (2), and (3) shown with arrows and paths are the system function options. First is the calibration mode which includes adjustment specs and design parameters. Second and third are open and closed loop operation modes. 37

Figure 3.4 **Intensity.** (a) Gaussian profile of light intensity in mW/cm^2, measured at 470nm (b) and (c) Top and side views. Effective section shown between red lines. (d) Light intensity adjustment scale. Line and dashed-line indicate sufficient and excess ranges. (e) Response profiles under four light intensity values: 1, 2, 3 and 4 mW/cm^2. Mustard colored bars represent normalized response amplitudes. Purple bars represent respond possibility of stimulated cells. (f) Characteristic responses summarized in (e). Typical time series shown in (f). Responses to 2, 1, and 3 mW/cm^2 light intensity stimulations are shown in top, middle and bottom rows respectively. 38

Figure 3.5 **Determination of optimal stimulation frequency and duty cycle.** (a) Four examples of frequency and duty-cycle optimization. From top to bottom, (i) to (iv). (i) continuous stimulation of 1.25s duration (ii) 25 ms period, 10 ms stim duration, packed in total 0.5 s with 20 pulses (iii) 50 ms period, 10 ms stim duration packed in total 1s with 20 pulses (iv) 100 ms period 20 ms stim duration packed in total 1s with 10 pulses (b) Stimulation pulse packets (c) Inter-spike intervals increase in continuous stimulation case. (d) Spike amplitudes decrease in high frequency and high duty cycles similar to the continuous stimulation case. 40

Figure 3.6 (a) Channel-rhodopsin expressing cells expressing tdTomato fluorescent. Dashed grid in white shows electrode positions at intersection points. (b) Scanning stimulation of 64 electrodes and neuronal responses. A synfire chain like task. (c) Post-Stimulus-Time-Histogram (PSTH) of selected channels which respond consistently. (d) Three groups assigned for poly-rhythmic stimulation shown in a bright field image. Black dots are electrodes and blue spots are stimulation light pulses. (e) Recorded responses of the three groups exhibit three distinct spike rates. 42

Figure 3.7 **Feedback.** Red and blue spots indicate the locations of event-detection and stimulation locations respectively. Blue arrowheads represent system flags. Dashed-line rectangles in red indicate detected events. Rate detection: Spikes detected in 100 ms bins. If more than two, an arbitrary threshold, spikes detected in the 100 ms intervals, it is assumed that the spike rate is increased. In response to that increase, system sets a flag, and actuates the stimulator. Coincidence detection: Spikes from two channels detected. If two spikes detected from two channels, within 10 ms intervals, it is assumed that a coincident event is detected. In response to that coincidence, system sets a flag, and actuates the stimulator. 43

LIST OF TABLES

Table 2.1 **Basic interaction profiles.**
A: Total number of neuron bodies on active electrode area (1 mm^2). B: Total number of candidate neuron bodies in ε-neighborhood. C: Number of primary neurons (directly stimulated neurons). D: Number of primary neurons that excite secondary neurons. E: Maximal distance between primary and secondary neurons. * Only significant values ($p<0.05$) included. 15

Table 2.2 **Multi-layered interaction profiles.**
(Only significant MPC scores ($p<0.05$) included). 23

Table 3.1 Electrical recording used with optogenetic stimulation. 45

Table 3.2 Closed-loop assays. 46

LIST OF SYMBOLS

r_{xy}	Cross correlation
c_{xy}	Pearson correlation coefficient
p_{xy}	p-value
σ_{xy}	Cross covariance

LIST OF ABBREVIATIONS

AAV	Associated adeno virus
AMPA	α-amino-3-hydroxy-5-methyl-4-isoxazolepropionic acid
AP5	(2R)-amino-5-phosphonovaleric acid
BDNF	Brain Derived Neurotrophic Factor
BSA	Bovine serum albumin
CaM	Calmodulin
ChR2	Channelrhodopsin-2
CNN	Cultured Neuronal Network
CNQX	cyanquixaline or 6-cyano-7-nitroquinoxaline-2,3-dione
CNS	Central Nervous System
DAPI	4',6-diamidino-2-phenylindole
DIV	Days-in-vitro
DLP	Digital Light Processor
DMD	Digital Micromirror Device
DRG	Dorsal Root Ganglia
EGFP	Enhanced Green Fluorescent Protein
FBS	Fetal bovine serum
GCaMP	Green CaM Protein
GCaMP6s	Sixth and slow version of GCaMP
GDNF	Glial cell line-derived neurotrophic factor
GECI	Genetically Encoded Calcium Indicator
GFP	Green Fluorescent Protein
ICC	Immunocytochemistry
LED	Light Emitting Diode
MEA	Multi Electrode Array
MPC	Mean Phase Coherence
NGF	Nerve Growth Factor
NMDA	N-methyl-D-aspartate

PBS	Phosphate-buffered saline
PFA	Paraformaldehyde
PNS	Peripheral Nervous System
ROI	Region of Interest
RPM	Revolutions per Minute
SLM	Spatial Light Modulator
SNR	Signal-to-Noise Ratio

1. INTRODUCTION

1.1 Background

1.1.1 Cultured Neuronal Networks

Utilization of *in vitro* neuronal cultures in neurobiology or neuroscience research constitute an essential part in understanding physiology of neurons. Cultured dissociated neurons develop neurites (axons and dendrites) and form connections that become circuits and networks. Healthy neuronal networks developed *in vitro* serve as platforms for studying neuronal interactions within assemblies. Neuronal cell cultures can be produced by using primary and secondary cells both having advantages and disadvantages. Origin of secondary cells is neuronal tumor lines and thus they exhibit physiological deviations from the concerned neuronal tissues. On the other hand, primary cells, post mitotic neurons, are assumed to keep resemblance with the neuronal tissue they are extracted from.

Primary cell cultures from many neuronal tissues can be produced but we are mostly interested in cortical and hippocampal tissues from central and dorsal root ganglia from peripheral nervous systems. Neuron types and their subtypes become varied from tissue to tissue, according to their function as well as their roles that they have in the circuits they are involved. Beside neurons, primary neuronal cultures also include other types of cells - a variety of glial cell types with proportions depending on tissue. Depending on the frame of the study, techniques and materials for neuronal cultures vary. For development of balanced and healthy networks *in vitro*, we prefer culture media and factors that promote neuron viability and activity.

Cultured neuronal networks are involved in plenty of application areas since they provide controllable environments for research before *in vivo* translation. Identification of various cellular mechanisms and cell-to-cell interactions under conditions of interest

can be studied using cultured neuronal networks thoroughly. As a matter of fact, much attention has been paid to neurotoxicity assays and pharmacological studies [1, 2].

Neurons exhibit spontaneous or stimulated activity in terms of action potentials that are measured through electrodes either intracellularly or extracellularly. Since the output of any application is composed of trains of spiking data obtained through single or multiple channels, deciphering neuronal network activity is indispensable. This fact directs the researchers to investigate neuronal activity (spontaneous and evoked) patterns both individually and in networks. At the same time, many studies have been devoted to improve understanding of neuronal representation, information handling and adaptation [3, 4, 5].

Activity patterns of the cultured neuronal networks exhibit differences according to their neuron type. For instance, cortical and hippocampal networks have intrinsic spontaneous activity with different characteristics [6]. On the contrary, although they form networks, dorsal root ganglia neurons are (almost) spontaneously silent in nature [7]. According to the application requirements neuronal type determines the framework for the research context. For many, a cultured neuronal network is assumed to represent a small-scale model of the brain or the neural tissue under investigation [8].

1.1.2 Multi and Micro Electrode Arrays

Bidirectional electrodes are essential tools to communicate living neuronal networks with electronic hardware and with digital platforms. They can be used both for recording and stimulation, where they transduce ionic currents to electronic currents and *vice versa* respectively. Use of micro machining technologies allows microelectrode designs in array and matrix configurations [9].

Since the cells are desired to adhere to surface in similar to the conventional glass bottom Petri dishes, *in vitro* electrodes are usually designed as planar to the glass substrate. There are alternate forms as well, such as needle-like electrodes or designs

that electrode positions are higher or lower than the plane, developed for research specific use. Interfacing neuronal signals requires amplification and data acquisition hardware as well. From late 70's to 00's, there was an era of transformation from analog to digital that it was, neither straightforward to get recordings from multiple channels, nor possible to carry out control over network activity. For *in vitro* multi electrode implementations, 8×8 matrix layout stands as a standard that in total makes a 64-channel interface. In general, although recording through all channels is convenient, limited number of channels are allocated for stimulation.

In case of a typical cultured neuronal network, recorded voltages are in the range of microvolts but stimulation voltages are in the range of volts. This 10^6 fold contrast in amplitude brings about practical troubles, such as the requisition of electrical separation and the electrical artifacts. There were efforts to overcome these issues both involving hardware and software, though a total removal did not seem to be attainable.

Since the diameter of an electrode is approximately 20 μm and a central nervous system neuron has an average diameter of 10 μm, it is likely to have multiple neurons in the close vicinity of an electrode. Therefore, electrical recordings of neuronal activity from a single electrode can include signals from more than one neuron. Since these signals as extracellular action potentials, are shaped according to the probed section of the neuron, it is possible to separate signals from individual neurons according to spike waveforms. Stimulation signals are created digitally and applied to the electrodes through either voltage or current controlled hardware. Stimulation waveforms can be created as monophasic or biphasic pulses, mostly biphasic pulses are preferred in order to minimize the risk of damage to the cells. Created pulses are repeated in trains with several different strategies such as theta burst stimulation or high frequency stimulation. Besides that, custom compositions of stimulation pulses are also widely used, depending on the research question.

1.1.3 Optogenetics

A relatively fresh approach has evolved for interfacing neuronal activity by means of optogenetics. In this method, cells in concern should be subjected to a genetic modification in order to make the cells produce a desired protein. To transfect the cell with a prepared plasmid, opening of a transient pore in the membrane is required from where the genetic material is inserted. To achieve this, techniques such as electroporation, chemical assistance and viral vector employment are prominent.

Although an artificially expressed protein can serve to any purpose that is desired, we focus on two approaches of the optogenetics. These can be concisely classified as neuronal activity monitoring and stimulation through light sensitive ion channels.

Neuronal activity monitoring issue intends to track voltage changes through fluorescent marked molecules using fluorescent microscopy. To observe voltage changes (action potentials) directly, a very high speed imaging camera is required, 500 to 1000 frames-per-second (fps) at least, in order to capture the events thoroughly. This approach is still in progress, depending on the related technological developments and their production rates. On the other hand, monitoring calcium transitions is more applicable because of its slower response profiles. Calcium activity is accepted as a surrogate for electrical activity, which provides a roughly low pass filtered expression of the spike data.

Genetically encoded calcium indicators (GECI) are tools available for tracking calcium transitions using the optogenetic approach. Among many GECI constructs, green calmodulin (CaM) protein (GCaMP) is the most widely employed calcium sensor. GCaMP incorporates green fluorescent protein (GFP), that is activated after calcium binding, and its emission wavelength is green under blue excitation. After calcium transitions are captured through fluorescent microscope, time-lapse analysis takes place on the high spatial resolution data. Resulting time-series output exhibits green fluorescent intensity changes (corresponds to calcium transitions) of a selected area which can be a cell body or an axonal section.

When it comes to the other way around, the second optogenetic tool that has our interest is light-activated opsins. Light sensitive ion channels are activated by specific wavelengths of light, channels open up for a definite period of time. Stimulation can either have excitatory or inhibitory action depending on the selected channel type. Although these channels comprise a large variety of different species, channel-rhodopsin-2 (ChR2) is the most known and the most used channel [10, 11].

ChR2 is a cation channel, activated by blue light, allows sodium ions to enter the neuron, which contribute to action potential generation. Blue light stimulation strategies commonly incorporate pulse trains, where the duration of individual pulses and the length of a pulse train depends on application framework. Although the kinetics of CHR2 is a well-studied issue, stimulation parameters like light intensity and pulse duration varies among experimental setups. The reason for these variations stems from the components employed in hardware setup, such as light source, light pathway and distance.

1.1.4 Integration of MEAs and Optogenetic Tools

Considering neuronal activity measurements as outputs and stimulation signals as inputs, a cultured neuronal network (CNN) can be thought as a model system or an *ex vivo* counterpart of the nervous tissue under investigation. To perform measurements and to stimulate the CNN in a designed assay, electrical techniques or optogenetic tools can be utilized. Use of electrical recording and electrical stimulation together bring about aforementioned drawbacks when simultaneous usage is required. Likewise utilizing optogenetic tools for both activity monitoring and stimulation have inherent technical disadvantages. To overcome handicaps of all-electrical and all-optical approaches, combinations or integrations of these techniques become reasonable.

These combinations or integrations can be realized in two directions, either using electrical stimulation with calcium imaging or optical stimulation with electrical recording. Both of these directions have advantages and disadvantages, both of which

can be preferable depending on the application.

In case of activity monitoring, electrical recording has high temporal but low spatial resolution. In contrast calcium imaging has just the opposite characteristics [12, 13]. When compared to electrical stimulation, optogenetic stimulation has unique properties [14]. Both excitatory and inhibitory stimulation choices are available with optogenetic technologies, as well as a cell-specific application capability [15].

As a result, depending on their individual qualities, two potential integration combinations might have different fields of application. The first approach, which involves combining calcium imaging with electrical stimulation, might be useful for investigating stimulation representations. In addition, participation of different cell types that comprise a network activity can be examined using this approach. The second approach, which integrates electrical recording with optogenetic stimulation utilizes the advantage of high temporal resolution activity monitoring in the presence of precise optogenetic stimulation. This combination might be useful in network adaption research where accurate spike timing and stimulation timing are required.

1.2 Outline

In this work we studied *in vitro* neuronal networks utilizing primary cell cultures obtained from mice. We used hippocampal and DRG neurons derived from new born and adult mice of type Balb-c. We grew these cultures on multi electrode arrays and applied optogenetic tools for both activity monitoring and optical stimulation purposes. Throughout our research, we developed two types of platforms that integrate MEAs with these features of optogenetics.

Platform type one incorporates electrical stimulation through MEAs and calcium imaging of GCaMP expressing neurons. In this first platform, we intended to use a spontaneously silent neuronal population, thus we employed DRG neurons. As a result, we conducted our research through stimulated activity, which allowed us to

observe network formation capabilities of dorsal root ganglia (DRG) neurons. We provided details of these experiments and their results in Chapter two.

In platform type two, we utilized optogenetics for stimulation, hence used ChR2 expressing hippocampal neurons. We carried out simultaneous electrical activity monitoring through MEAs and local optical stimulation. For local optical stimulation we employed a high resolution digital micromirror device (DMD) based projection approach equipped with a bright field microscope. We illustrated how this platform may be used to address the drawbacks of earlier techniques. In Chapter three, we presented these findings.

2. PLATFORM I: ADULT MOUSE DORSAL ROOT GANGLIA NEURONS FORM ABERRANT GLUTAMATERGIC CONNECTIONS IN DISSOCIATED CULTURES

Cultured sensory neurons can exhibit complex activity patterns following stimulation in terms of increased excitability and interconnected responses of multiple neurons. Although these complex activity patterns suggest a network-like configuration, research so far had little interest in synaptic network formation ability of the sensory neurons. To identify interaction profiles of Dorsal Root Ganglia (DRG) neurons and explore their putative connectivity, we developed an *in vitro* experimental approach. A double transgenic mouse model, expressing genetically encoded calcium indicator (GECI) in their glutamatergic neurons, was produced. Dissociated DRG cultures from adult mice were prepared with a serum-free protocol and no additional growth factors or cytokines were utilized for neuronal sensitization. DRG neurons were grown on microelectrode arrays (MEA) to induce stimulus-evoked activity with a modality-free stimulation strategy. With an almost single-cell level electrical stimulation, spontaneous and evoked activity of GCaMP6s expressing neurons were detected under confocal microscope. Typical responses were analyzed, and correlated calcium events were detected across individual DRG neurons. Next, correlated responses were successfully blocked by glutamatergic receptor antagonists, which indicated functional synaptic coupling. Immunostaining confirmed the presence of synapses mainly in the axonal terminals, axon-soma junctions and axon-axon intersection sites. Concisely, the results presented here illustrate a new type of neuron-to-neuron interaction in cultured DRG neurons conducted through synapses. The developed assay can be a valuable tool to analyze individual and collective responses of the cultured sensory neurons.

2.1 Introduction

Sensory neurons innervate internal and external organs and transmit noxious and non-noxious information to the Central Nervous System (CNS). They are pseudo-unipolar cells with axons bifurcating into two distinct branches, one extending to peripheral receptors and the other to the spinal cord [16]. Action potentials generated in sensory receptors travel from the peripheral to the central processes of Dorsal Root Ganglia (DRG) neurons, without passing through any synaptic connections [17, 18, 19]. Sensory neuron bodies located in the DRG are thought to behave like rarely depolarizing passive units, where afferent signals bypass the neuron bodies and continue to the CNS [20]. In contrast, DRG neurons typically exhibit complex neuron-to-neuron interactions and ectopic discharges emerge from their somata in cases of injury, inflammation, or strong excitation [18]. Despite being studied extensively in many platforms within varying contexts, the reason for these neuron-to-neuron interferences inside a ganglion is not clearly understood. To our knowledge, very little research so far had been carried out concerning synaptic formation and network development potentials of sensory neurons. In this work, we wanted to examine whether DRG neurons could develop functional connections through synapses and form circuits with each other *in vitro*. For this purpose, we studied response profiles and communication among DRG neurons *in vitro* using a multimodal approach. We used local extracellular electrical stimulation through MEA electrodes and GECI-based calcium monitoring, simultaneously.

Since most DRG neurons are excitatory and glutamate is a major excitatory transmitter in peripheral and central nervous systems [21], we examined neuronal communication through glutamatergic synaptic function. Consequently, we used adult DRG neurons of a custom double transgenic mouse model, expressing GCaMP6s at its glutamatergic neuron bodies. We employed modality-free electrical stimulation and visualized spontaneous and stimulus evoked calcium (Ca^{2+}) activity at cell bodies of GCaMP6s expressing DRG neurons via confocal microscopy. An almost single-cell level stimulation was achieved by adjusting the confluency of cultures grown on MEAs.

In vitro models, allowing visualization and manipulation of both neuronal and glial cells, are potent tools for providing information at various scales. The use of MEAs allows network level investigations of neuronal populations [22, 23, 24]. However, in DRG culture assays incorporating MEA platforms, certain limitations arise. The DRG neurons exhibit spontaneous activity in sub-threshold voltage levels which is hard to decipher with standard extracellular measurements. Cytokines and growth factors have been used conventionally to sensitize neural populations [25, 26] to obtain spontaneously active DRG neurons. However, our multimodal approach does not require additional factors or cytokines. In addition, calcium imaging enables the observation of sub- and supra-threshold calcium transients with high spatial resolution. Genetically encoded calcium indicators (GECIs) enable monitoring calcium dynamics of neuronal populations for a theoretically unlimited amount of time, in a non-invasive fashion with high signal-to-noise ratio (SNR) [27, 28]. The GECI constructs can be targeted to specific cell types [29].

In this study we present an experimental approach for identifying interaction profiles of DRG neurons in an *in vitro* setting. We describe, for the first time, a synaptic network formation in cultured DRG neurons and demonstrate that synaptic formation has an important role in the emergent correlated activity. Our results indicate that the correlated activity is totally suppressed by post-synaptic glutamatergic antagonists. When immunocytochemistry (ICC) is applied, synapse formation is further demonstrated by the presence of presynaptic protein marker, synaptophysin. Synapses are observed mainly in axonal terminals, axon-soma junctions, and axon-axon intersection sites. Understanding the neuron-to-neuron interaction mechanisms as described here will improve our perception on sensory neuron functioning and may lead to new, effective clinical and pharmacological studies on sensory neuron disorders.

2.2 Methods

2.2.1 Ethics statement and animal handling

Transgenic mice strains were kept and bred in *The Experimental Animal Center of Istanbul Medipol University*. All animals were handled in strict accordance with guidelines for animal care and use issued by the EU directive code; 86/609/CEE. *The Committee on Ethics of Animal Experimentation of Istanbul Medipol University (IMUHADYEK)* approved all procedures. Two transgenic mice strains purchased from Jackson Laboratories were used. The first one was a knock-in strain Vglut2-ires-cre (C57BL/6J), having Cre-recombinase enzyme expression in excitatory glutamatergic neuronal cell bodies. The second was Ai96 (RCL-GCaMP6s), a Cre-dependent calcium indicator strain (C57BL/6J), which emits EGFP fluorescence after calcium binding. These two original strains were crossbred and the offsprings successfully expressed GCaMP6s in their glutamatergic neurons. In total, six transgenic animals were used in the present work.

2.2.2 Dissociated DRG culture protocol

The dissociated adult DRG culture protocol was adapted from a previously published work [30]. Prior to the dissection, mice were euthanized with CO_2 asphyxiation and rapid decapitation. In a sterile hood, ganglia were collected in the *Dissection Medium*. Collected ganglia were transferred into the *Enzyme Solution 1*, and incubated in 37°C, 5% CO_2 for 40 minutes. Then, the ganglia were washed with Hank's Balanced Salt Solution, (HBSS, Sigma) and transferred into *Enzyme Solution 2* for 15 minutes at 37°C, 5% CO_2 incubation. Following the incubation in *Enzyme Solution 2*, the ganglia were gently triturated with pipettes of decreasing diameters (1.32 mm, 1.0 mm, 0.83 mm, 0.45 mm). After the trituration step, the cell suspension was diluted within the *Enzyme Inhibition Medium* to remove enzyme activity. To maximize the neuron yield from the mixed cell population and the debris, a cell purification step was incorporated using a three-layer *Percoll Gradient*. Cell suspension was layered on *Percoll Gradient*

gently and spun at 1700 RPM at 4°C. Cells collected from the middle layer were plated with an average density of 100 cells/mm^2 using 4.7 mm diameter cloning cylinders (Sigma). Half of the maintenance medium was reloaded every three or four days to maintain the viability of the cells up to two months. The details of the preparations and the contents of all the solutions and the media used in our experiments are given in Appendix A.

2.2.3 Immunocytochemistry

An MEA plate was fixed on the day of experiment (Table 1, Plate 8) with 4% paraformaldehyde (PFA, pH 6.9) and washed gently with phosphate buffer saline (PBS, Sigma). Blocking and permeabilization of the cells were performed using the *Blocking Solution*. Afterwards, a second wash was performed, and preparation was incubated with primary antibodies in the *Dilution Solution*, overnight at 4°C. Utilized primary antibodies were chicken Anti beta-III Tubulin (Abcam) and rabbit Anti-Synaptophysin (Santa Cruz) with 1:200 and 1:50 dilutions, respectively. After that, the primary antibodies were washed out with PBS and secondary antibodies were added and incubated for three hours at room temperature. Secondary antibodies were Alexa Fluor 633 goat anti-chicken Immuno-globulin-G (IgG) and Alexa Fluor 488 goat antimouse IgG (Invitrogen) with 1:100 and 1:400 dilutions, respectively. DAPI (Invitrogen) was added to the sample at 1 μg/ml concentration. A final wash with 2:1000 PBS-Tween20 solution was performed in dimmed light and preparation was kept in PBS-Azide with 1:1000 dilution.

2.2.4 Preparation of MEAs

MEAs with 64 planar microelectrodes etched to 5cm×5cm glass substrates were purchased from *The Center for Network Neuroscience* of the *University of North Texas*. We removed the glass bottoms of standard 35mm Petri dishes and adhered the remaining polystyrene frames to the MEAs using a medical adhesive (Hollister- 7730). The

new MEA dishes were sterilized with 3% bleach and 70% ethanol and placed under UV light for two hours in a laminar flow hood. Afterwards, they were coated with 0.1% polyethyleneimine (PEI, Sigma) solution prepared in 0.1M borate buffer for two hours and rinsed off thoroughly with sterile de-ionized water. The dishes were then coated with 40 ng/mm^2 Laminin (Sigma) diluted in double-distilled water (dd-H_2O) and kept at 37°C incubation overnight.

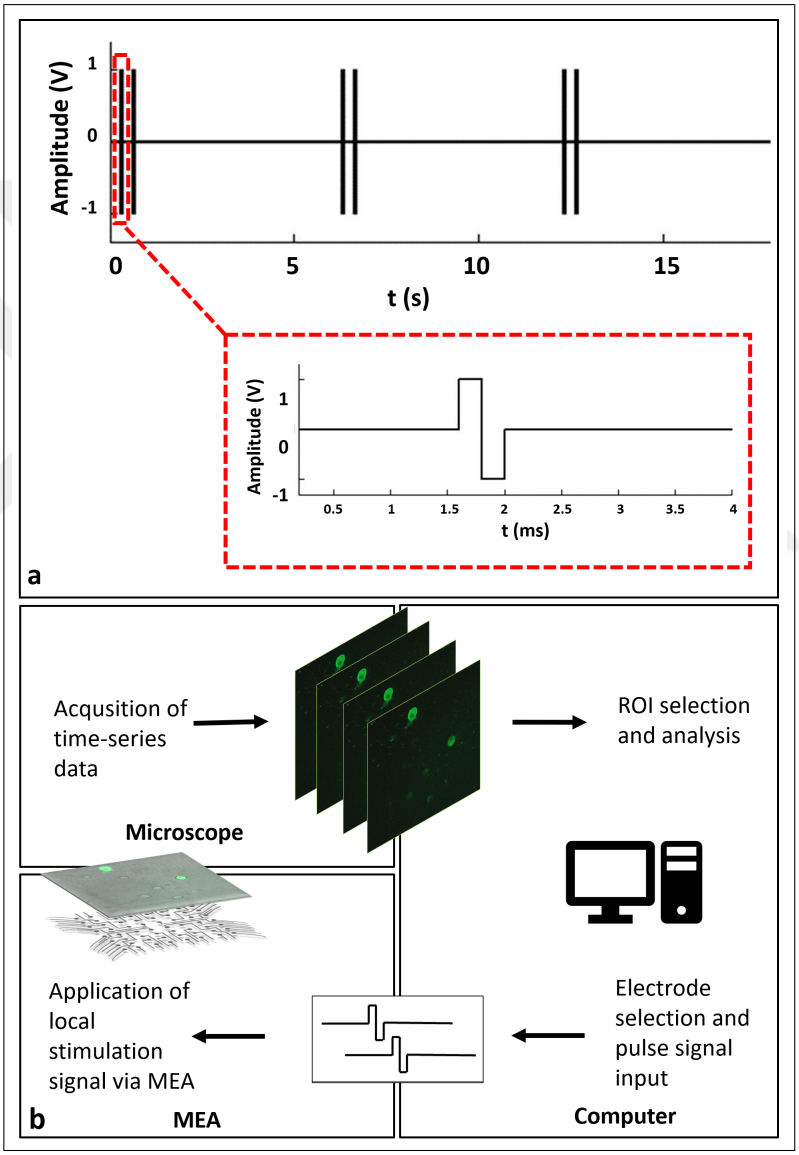

Figure 2.1 a: A typical stimulation strategy. A stimulation consists of two biphasic pulses of 400 μs duration, repeated in 0.5 s. Stimulation is repeated within six second periods. **b: Schematic representation of the experimental procedure.** Timelapse imaging and electrical stimulation of GCaMP6s expressing neurons using a MEA headstage placed on an inverted fluorescent microscope. Acquisition of calcium responses and live monitoring. Offline event detection, analysis and rendering of analog voltage signals.

2.2.5 Local electrical stimulation

The electrical stimulation hardware consisted of an MEA interfacing headstage, a digital to analog conversion board, a router circuitry, and a controlling PC (Lenovo). Plexon MHP64 headstage was used for interfacing MEAs which was designed for the 64 channel MEA layouts. A custom designed router circuitry was employed for directing analog stimulation signals to selected channel or channels from 64 alternatives. Digital stimulation signals were converted to analog voltages using National Instruments (NI) 6001 board, at a sampling rate of 5 kHz. Digital to analog conversion and router circuitry were controlled with a custom software written in MATLAB (Mathworks Inc.) incorporating Data Acquisition Toolbox (Mathworks Inc.) and utilizing the NI drivers and libraries. All stimulation signals were voltage controlled biphasic pulses and the stimulation parameters were adapted from previous studies [31, 32, 33]. The pulse durations and the amplitudes that elicited stable and reproducible responses were empirically adjusted in the ranges of 100-500 μs and 1-3 V, respectively.

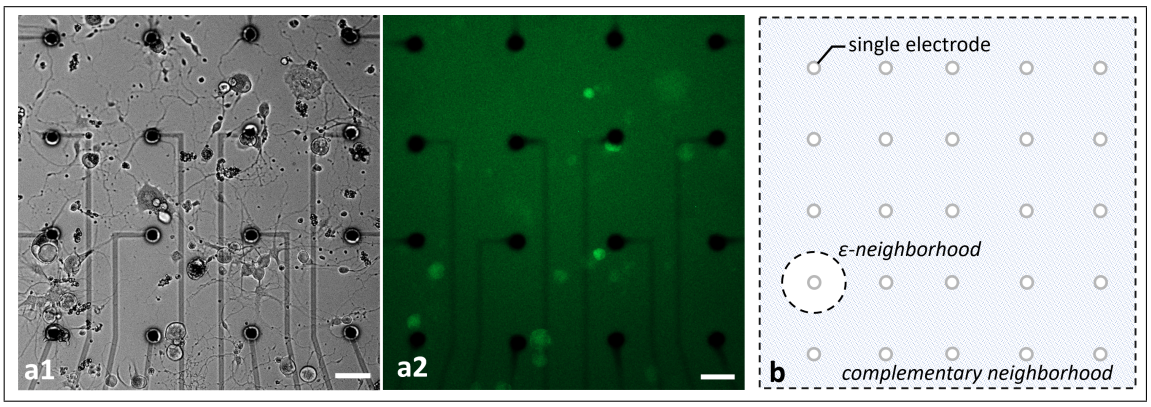

Figure 2.2 Phase contrast (a1) and fluorescent (a2) images of typical cultures of DRG neurons. The cultures were grown on MEA plates with an average density of 100 cells/mm2. Fluorescent image shows the GCaMP6s expression of transgenic glutamatergic neurons at DIV3. Scale bar: 50 μm at 10x magnification. The illustration of ε- and complementary neighborhood definitions (b).

2.2.6 Experimental procedure

To observe individual calcium responses clearly, the stimulation period was selected as six seconds, similar to previous studies [33, 34]. Within six second periods, stimulation was applied as dual-pulses in 2 Hz. After the candidate electrodes were determined, the scanning stimulation pulses were applied to each candidate electrode in sequence. In this way, the regions that respond to stimulation were selected. A typical stimulation strategy that was used in the experiments is shown in Figure 2.1(a). The MEA headstage was placed on a custom-made heating unit, similar to a previously reported interface on an inverted confocal microscope stage (Carl Zeiss, Cell Observer) [35]. Time lapse images were acquired simultaneously while applying local electrical stimulation through selected electrodes. For imaging, a 10× Plan Apochromat objective and a 488 nm excitation wavelength laser were used along with a 500-550 nm emission filter. Image acquisition was performed at an average rate of three frames per second which sufficiently captured GCaMP6s dynamics [33]. A schematic diagram of the experiment loop can be seen in Figure 2.1(b). All experiments were carried out with identical stimulation set up in *default (non-blocked)* and *blocked* conditions where NMDA, AMPA and Kainate receptor blockers were applied to the cultures.

Table 2.1
Basic interaction profiles.
A: Total number of neuron bodies on active electrode area (1 mm^2). B: Total number of candidate neuron bodies in ε-neighborhood. C: Number of primary neurons (directly stimulated neurons). D: Number of primary neurons that excite secondary neurons. E: Maximal distance between primary and secondary neurons. * Only significant values ($p<0.05$) included.

	Plate1	Plate2	Plate3	Plate4	Plate5	Plate6	Plate7	Plate8
A	52	43	54	74	50	53	49	62
B	33	27	10	51	14	10	13	23
C*	5	4	3	5	6	5	4	5
D*	3	3	2	4	3	2	2	3
E (μm)	1000	860	730	800	920	900	600	700

2.2.7 Image analysis and statistics

Neuronal cell bodies were selected as regions of interests (ROIs) manually using Fiji software [36]. A selected set of ROIs and the corresponding stimulation electrode was assigned as an individual experiment. Each pixel that a region encloses, was assumed to have a uniformly distributed variation in light-intensity and calcium activity of each neuronal unit was calculated by averaging. Then the relative change of light intensities, $\Delta F/F(t)$, were computed for each ROI after subtracting the background [37]. In order to eliminate imaging noise and to remove the out-of-range frequency components, a moving-average filter was applied to each time-series [38].

To evaluate the similarity between the responses of the selected ROIs, cross-correlation analysis was applied to each pair of time-series. To obtain a consequent output, a cross-correlation measure for any two time-series, the cross-covariance was computed using Eq. 2.1 and Eq. 2.2,

$$\sigma_{xy}(T) = \frac{1}{N-1}\sum_{t=1}^{N}(x_{t-T} - \mu_x)(y_t - \mu_y) \tag{2.1}$$

$$r_{xy}(T) = \frac{\sigma_{xy}(T)}{\sqrt{\sigma_{xx}(0) \cdot \sigma_{yy}(0)}} \tag{2.2}$$

where N is the length and, μ_x and μ_y are mean values of time series x and y respectively.

The maximum values of the cross-correlation signals were determined, allowing a maximal lag of a stimulation period. Then using lag-compensated cross-correlation results were further processed to find Pearson correlation coefficients with Eq. 2.3,

$$c_{xy} = \frac{N(\sum xy) - (\sum x)(\sum y)}{\sqrt{[N\sum x^2 - (\sum x)^2][N\sum y^2 - (\sum y)^2]}} \tag{2.3}$$

The correlation coefficients above a selected threshold were used in connectivity analyses, and their significance was determined using p-value statistics calculated using Eq. 2.4,

$$p_{xy} = c_{xy}\sqrt{\frac{N-2}{1-c_{xy}^2}} \tag{2.4}$$

To group the calcium responses hierarchically, city-block distance and complete link clustering algorithms were employed. In addition, a phase synchronization index, *Mean Phase Coherence* (MPC), was employed for determining phase coupling strength of the correlated calcium responses [39]. To compute the MPC values, instantaneous phase differences of the time-series were utilized as follows (Eq. 2.5),

$$MPC_{xy} = \mid \frac{1}{N}\sum_{j=0}^{N-1} e^{i\phi_{x,y}(j\Delta t)} \mid \tag{2.5}$$

2.3 Results

Healthy populations of adult DRG cells were obtained with a high viability ratio of 90-95%. The cells firmly attached on the MEA surfaces due to the optimized coating protocol. Neurite elongation was observed in the first hour of plating. Plated cell populations included 60-65% of the neurons, the remaining were glial cells. Figure 2.2 shows phase contrast (a1) and fluorescent images (a2) of a typical DRG culture grown on an MEA dish. A high-throughput expression of GCaMP6s can be seen on glutamatergic neurons at the third day *in vitro* (DIV3). All the experiments were conducted between DIV2-11. Glutamate receptor antagonists were used for examining

postsynaptic connections between the DRG neurons [40]. In the presence of NMDA, AMPA and Kainate receptor blockers, synaptic communication ceased completely. Induced calcium activity patterns changed dramatically when the glutamatergic synapses were blocked. The results were verified with post-control data, obtained after the wash out of the chemical antagonists with fresh media. Experimental steps are outlined in Figure 2.3.

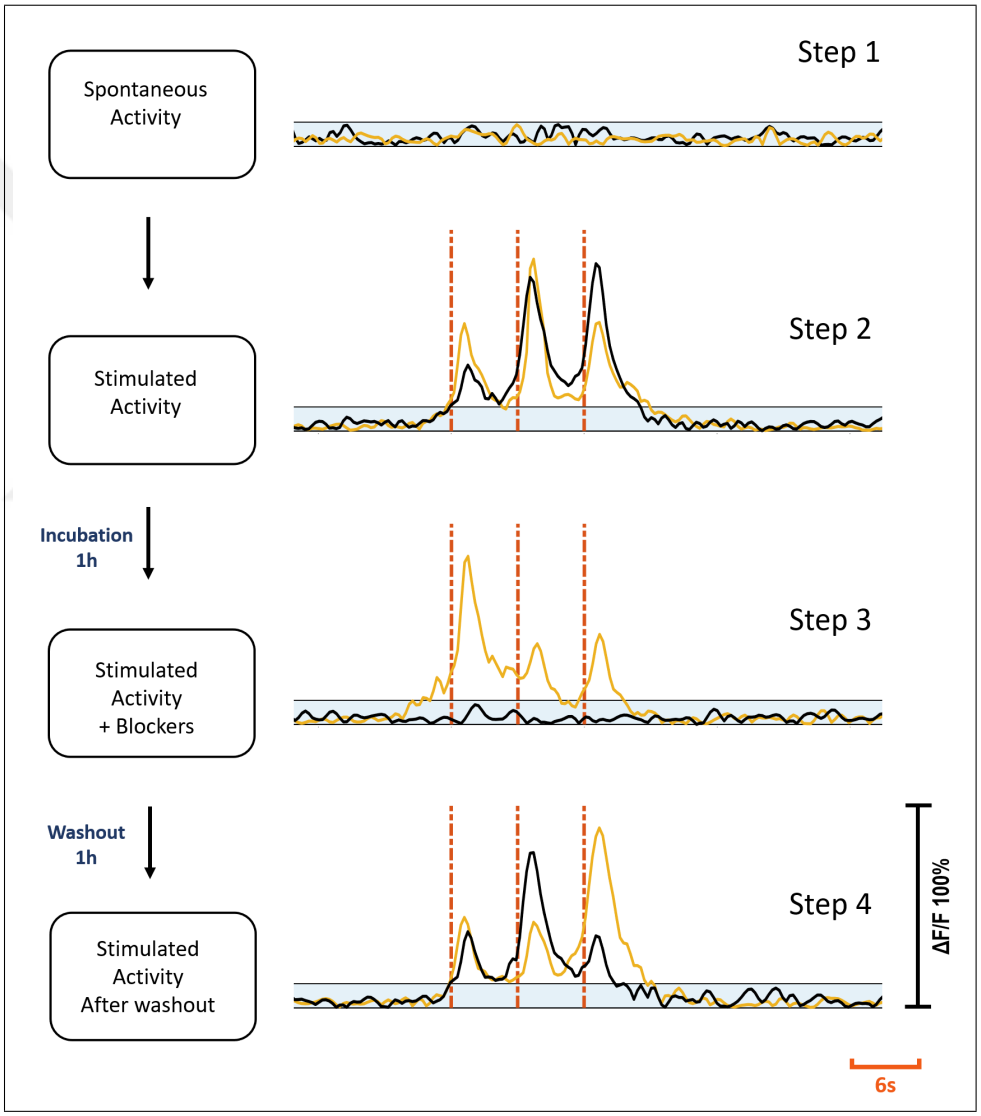

Figure 2.3 Experimental steps. Step one: Spontaneous activity recording prior to stimulation. Step two: electrical stimulation applied. Step three: Stimulation repeated after cultures were treated with blockers for 1h. Step four: Stimulation repeated after washout and 1h incubation. Yellow and black traces show activities of the same c^+ and c^- primary neuron at each step respectively. Blue shaded areas show subthreshold. Red dashes show stimulation instants. Each stimulation trace corresponds to a 2 Hz dual-biphasic pulses repeated in 6 sec periods. Vertical axis shows normalized $\Delta F/F(t)$.

Active MEA areas, approximately a total of 1 mm^2 region, were monitored with a 10× objective and the total number of neuronal bodies were counted (Table 2.1, row A). *Primary Neurons* were defined as the neuron bodies which were directly stimulated by an electrode. A circle of radius ε around each selected electrode, called a ε-*neighborhood*, was determined to be the area where primary neurons reside. *Secondary Neurons* were defined as the neurons which were excited by the primary neurons. They were observed throughout the active MEA area outside the ε-*neighborhood*, called the *complementary neighborhood*. An illustrative diagram for neighborhood definitions can be found in Figure 2.2(b).

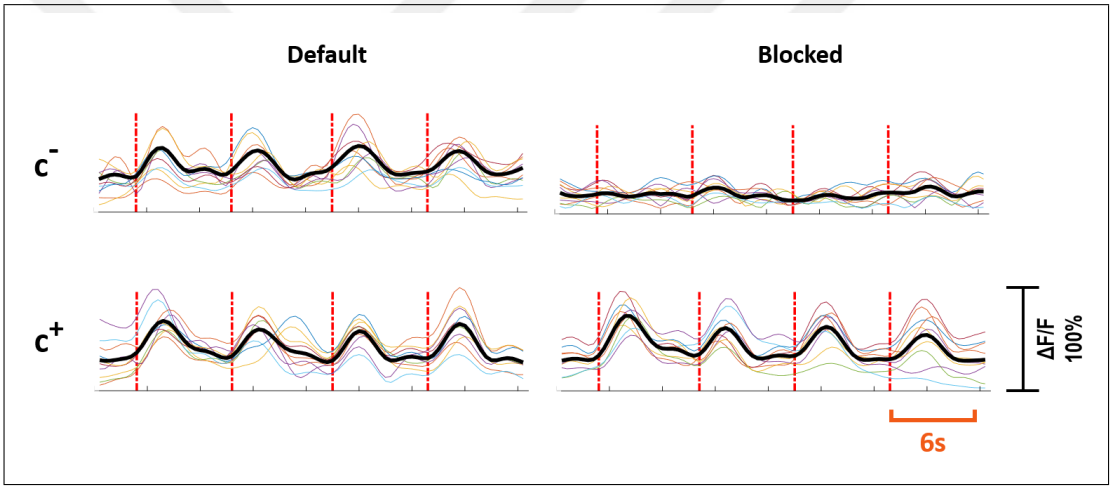

Figure 2.4 Response profiles of c^+ and c^- neurons. Individual experiments are shown in color and the averaged response is shown in black. The first row shows the responses of c^- neurons and the second row shows the responses of c^+ neurons. The left and right column shows responses to stimulation in default and blocked cases, respectively. Red dashed lines show stimulation instants. Stimulation period is six seconds. Vertical axis shows normalized $\Delta F/F(t)$.

In the reported experiments, we selected the neighborhood parameter as, $\varepsilon = 50$ μm. Table 2.1 summarizes the basic interaction profiles of each MEA plate. Out of a total of 437 neurons in the active areas of these eight MEA plates (Table 2.1, row A), 181 were in the ε-neighborhood (Table 2.1, row B). These neurons in the ε-neighborhood were defined as *candidates* for primary neurons. To determine the primary neurons, we stimulated the candidates via selected electrodes in the ε-neighborhood. A total of 37 candidate neurons responded to the stimulation ($p<0.05$) and they were labeled as the primary neurons (Table 2.1, row C). Out of these 37 primary neurons, 22 were found

to excite at least one other neuron (60% ± 15.7 with a confidence interval of 95%, $p<0.05$) (Table 2.1, row D). The neurons that were excited by the primary neurons were the secondary neurons. The last row of Table 2.1 shows the maximal distances between primary and secondary neurons.

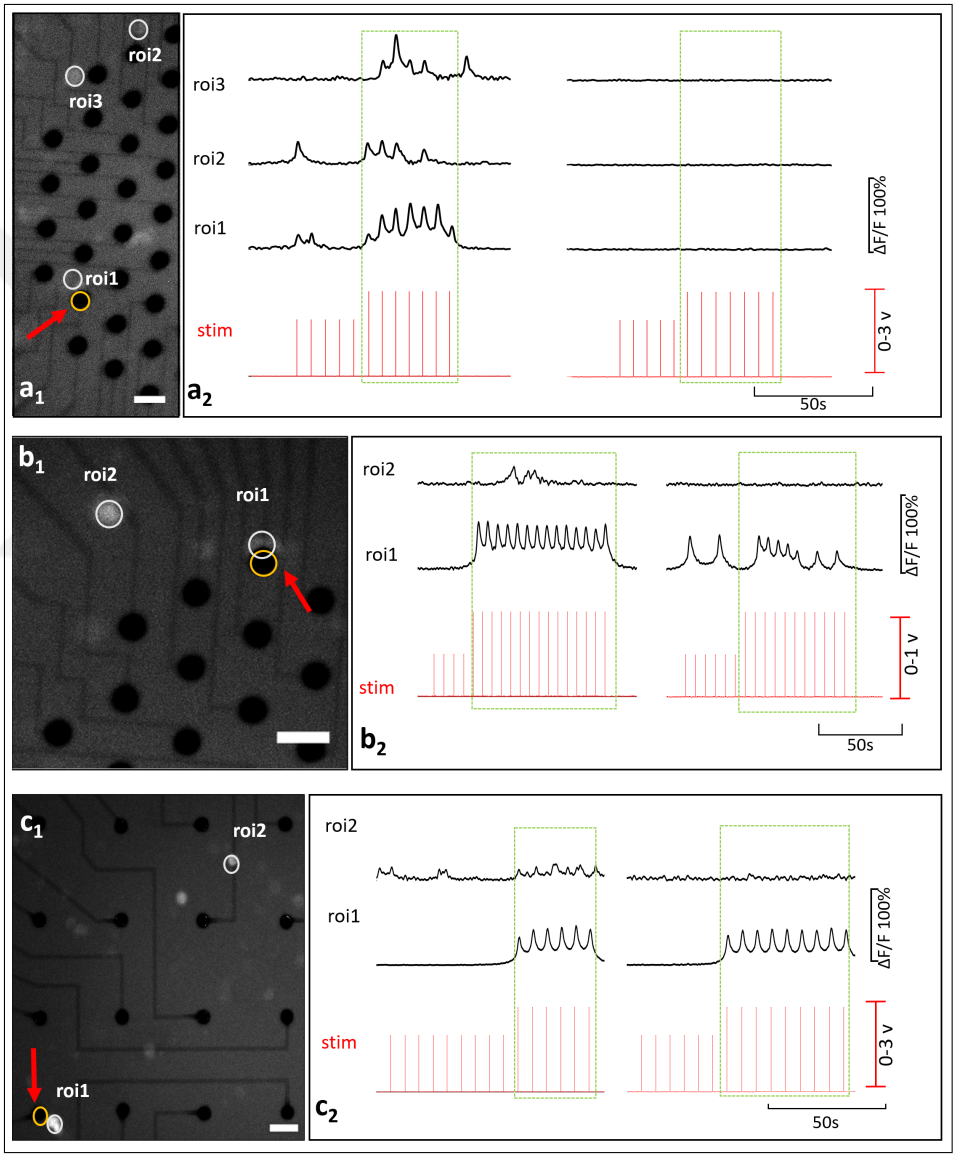

Figure 2.5 Basic interactions. (a) is an example for a c^- primary neuron and (b) and (c) are for c^+ primary neurons. Secondary neurons in (b) and (c) represent previously silent and previously spontaneously active types respectively. Fluorescent images show the locations of the stimulation electrode and the neuron bodies in a1, b1, and c1 (Scale bar: 50 μm, magnification: 10×). Stimulation instants and the corresponding time-series of calcium activity recorded in absence (left) and presence (right) of glutamatergic antagonists, a2, b2, c2.

Two distinct response profiles were observed depending on the presence and the absence of a contact between the stimulation electrode and the primary neuron. If a direct contact was present, it was defined as the *c^+ primary neuron* and if there were no direct contact it was defined as the *c^- primary neuron*. Out of 37 primary neurons, 21 (57%) were of c^+ type, and 16 (43%) were of c^- type. For the c^+ primary neurons, synaptic blockers did not impede the evoked responses. However for the c^- primary neurons, the evoked responses were suppressed with blocker application. Figure 2.3 shows the characteristic response profiles obtained from c^+ and c^- type primary neurons at each experimental step. The responses of each c^+ and c^- primary neuron ($n = 13$ for c^+, $n = 10$ for c^-) recorded in default and blocked conditions can be seen in Figure 2.4.

2.3.1 Stimulated neuronal responses activate other neurons via glutamatergic connections

Interaction profiles between primary and secondary neurons are illustrated in Figure 2.5, for both c^- (a) and c^+ type primary neurons (b and c). In Figure 2.5(a), the c^- primary neuron (ROI 1) excites two secondary neurons (ROIs 2 and 3). Locations of these neurons and the stimulation electrode can be seen from the fluorescent image presented in Figure 2.5(a1). Recorded Ca^{2+} responses of these primary and secondary neurons are shown in Figure 2.5(a2). Correlation analysis confirmed that the secondary neurons were excited by the c^- primary neuron ($p<0.05$). In the blocked condition, no Ca^{2+} activity was observed.

Although the induced Ca^{2+} activity persisted under the glutamatergic inhibition for c^+ primary neurons, excitability of the secondary neurons discontinued. Secondary neurons exhibited two common excitation profiles depending on whether they were silent or spontaneously active before stimulation. These two profiles were encountered in equal frequencies 30% (both 7 out of 22) all throughout the experiments. In Figure 2.5(b), the c^+ primary neuron was observed to excite a previously silent secondary neuron. In the blocked case this excitation was not observed as shown via correlation

analysis ($p<0.05$). Figure 2.5(c) shows an example for a secondary neuron which was spontaneously active before stimulation. Spontaneous activity of the secondary neuron was modulated with the induced Ca^{2+} activity of the primary neuron. Excitation of the secondary neuron continued through the stimulation and the in-phase modulation vanished in the blocked case ($p<0.05$).

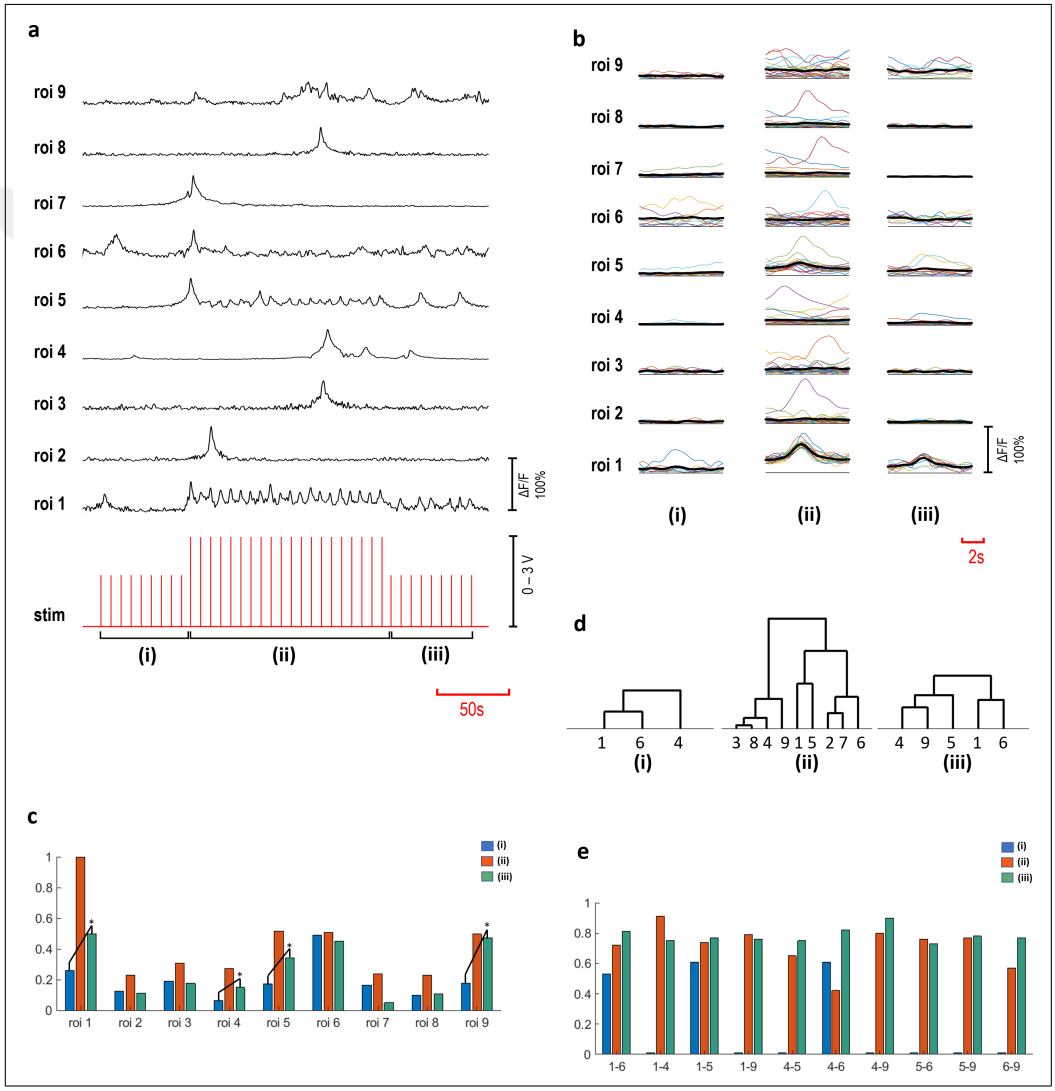

Figure 2.6 Multi-layered interactions. Time-series of ROIs 1-9, ROI 1 is a c- primary neuron and ROIs 2-9 are secondary neurons (a). The stimulation voltage applied in three steps (2V-3V-2V) indicated as (i, ii, iii). (b) shows the averaged responses to individual stimuli detected in three voltage steps (n = 10 for (i) and (iii) steps, n = 20 for (ii) part). Response amplitude alterations are shown in normalized averaged values (c). Response amplitudes of ROIs 1, 4, 5 and 9 increased significantly from step (i) to (iii) ($p<0.05$). Hierarchical groups are shown, based on significant correlations ($p<0.05$) (d) and the connectivity strength values calculated with significant MPC scores ($p<0.05$), (e) obtained from connectivity analyses.

2.3.2 Higher order synaptic interactions

Increasing the confluency of the cultures produced rather complex interaction patterns between neuronal activities. A complex interaction scheme is presented in Figure 2.6, where a c^- primary neuron excites eight secondary neurons. In the blocked repetition of the experiment, interaction between the primary and the secondary neurons disappeared ($p<0.05$). Recorded Ca^{2+} activities of these neurons are shown in Figure 2.6(a), as $\Delta F/F(t)$ time-series. A stimulation strategy involving three amplitude (voltage) steps (2V-3V-2V) was employed in order to investigate the effect of the successive stimulation on neuronal excitability. Figure 2.6(b) shows the acquired responses to each stimulus for three voltage steps, indicated as (i, ii and iii).

Table 2.2
Multi-layered interaction profiles.
(Only significant MPC scores ($p<0.05$) included).

	i	ii	iii
ROIs 1-6	0.61	0.74	0.77
ROIs 1-4	0.53	0.72	0.81
ROIs 1-5	–	0.91	0.75
ROIs 1-9	–	0.79	0.76
ROIs 4-5	–	0.65	0.75
ROIs 4-6	0.61	0.42	0.82
ROIs 4-9	–	0.80	0.90
ROIs 5-6	–	0.76	0.73
ROIs 5-9	–	0.77	0.78
ROIs 6-9	–	0.57	0.77

A summary of the averaged and normalized responses is presented in Figure 2.6(c). Significant increase in the excitability of ROIs 1, 4, 5 and 9 was observed ($p<0.05$) and shown with asterisks. Furthermore, we investigated connectivity, using cross correlation and MPC analyses, separately for the three stimulation periods (i, ii,

iii). Significant connections are illustrated as hierarchical trees, shown in Figure 2.6(d) ($p<0.05$). In these three stimulation periods, network structures varied through lower orders of hierarchical connections. Connected pairs that were common in these stimulation periods were then investigated in terms of the connectivity strengths. Significant alterations in the functional connections are summarized in Table 2.2 and Figure 2.6(e) ($p<0.05$).

2.3.3 Structural verification of synapses

To examine synaptic formations on MEA plates, immunostaining was performed (Table 2.1, Plate 8). Synaptophysin staining was observed among almost all the tubulin positive neurons, prominently concentrated in three distinct regions. These three regions were axon terminals, soma-axon contact sites and axon-axon intersection points. These regions may correspond to synapse types commonly described as, axo-extracellular, axo-synaptic, axo-somatic and axo-axonic (Figure 2.7). Figure 2.7(1) and (2) show a soma-axon connection and an axon terminal, respectively. The axon-axon intersection sites were observed to be widespread. The a, b, c and d labels show tubulin in red, synaptophysin in green, DAPI (blue-fluorescent DNA stain) and brightfield channels respectively.

2.4 Discussion

In this study, we investigated cultured DRG neurons in terms of their spontaneous and induced electrical activity patterns and searched whether they developed networks with each other. For this purpose, we developed an experimental platform combining fluorescent imaging and local electrical stimulation of GCaMP6s expressing sensory neurons from adult mice. We have shown that correlated activity in cultured DRG neurons originate from network formation. Network events were successfully addressed to glutamatergic synapses which were detected in the axonal terminals, axon-soma junctions and axon-axon intersection sites in almost all neurons. Studies using a

multi-modal experimental approach to understand interaction profiles of DRG neurons *in vitro* are rare and to our knowledge, no study on DRG networks has been reported previously.

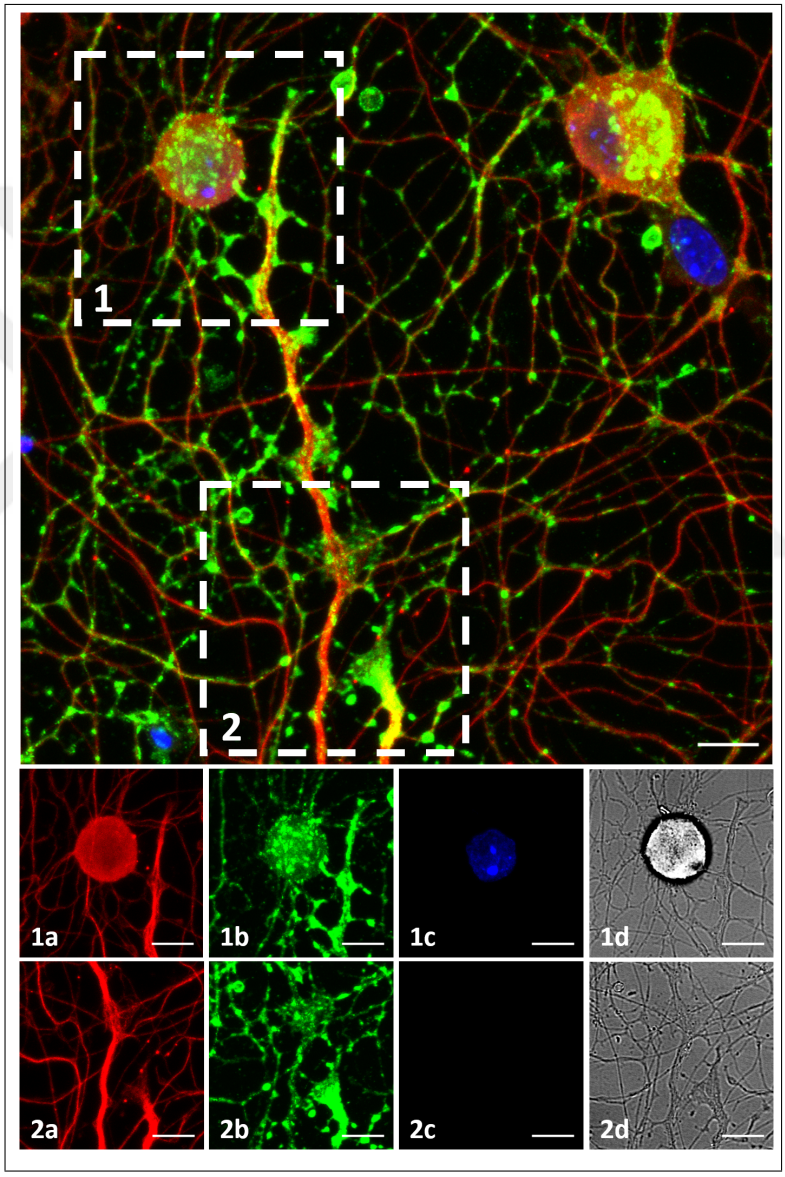

Figure 2.7 Immunocytochemistry. DRG culture on a MEA plate fixed on DIV3. Top: Figure shows maximum intensity projection of 14 z-stack images acquired in various depths, merging 3 channels. β-III Tubulin is shown in red, Synaptophysin is shown in green and DAPI is shown in blue. Bottom: (1) and (2) show a soma-axon connection and an axon terminal in detail. The axon-axon intersection sites are observed widespread. The a, b, c and d labels showtubulin, synaptophysin, DAPI and brightfield channels. Objective: 40×, scale bar:10 μm.

The culture protocol for dissociated DRGs from adult mice with a serum-free protocol provided high viability rates and adequate conditions for growth and development of neurons. Also, the gradient-based cell sorting process resulted in seeding of a low percentage of glial cells with a high neuronal population compared to previous studies. Avoiding the need for anti-mitotic agents by using an optimized culture medium for neurons [41], we reduced the stress and improved the life span of the cultures. To evoke spontaneous electrical and calcium activity in DRG cultures, use of growth factors and cytokines such as NGF, BDNF or GDNF is a common practice [25, 26]. However, synthetic sensitization of the neurons may bring unexpected interactions [42, 43]. Cheng et al. found out that elevation in NGF levels builds up synapse-like structures between sprouted neurites, resulting in mechanical hypersensitivity of healthy neurons [44]. Accordingly, to preserve physiological activity profiles as much as possible, we did not resort to inflammation models for sensitization.

Electrical and optical techniques together were used by Wainger et al. for tracking the activity of nociceptor neurons re-programmed from fibroblasts in order to develop a model for pain research [45]. Following that, Enright applied simultaneous Fluo-8 imaging with MEA recording for investigating primary human DRG neurons exposed to chemical stimulants [46]. Fluo-8 has a better temporal resolution compared to the GECIs. However they are nonselective, run for limited durations of time and require strict dye-loading protocols [47]. In our approach, we used a targeted GECI to track only the glutamatergic DRG neurons, since glutamate is the presumed neurotransmitter between the DRG and the spinal cord [48]. Vesicular glutamate transporters vGLUTs, found in glutamatergic neurons, can be employed for targeting and identification of DRG neurons, particularly the vGLUT-2 subtype which is found broadly and expressed more in medium to small, nociceptive neurons [40, 49]. The animal model we used ensures correct identification of GCaMP6s expressing vGLUT-2 positive DRG neurons.

The stimulation protocols used in previous works were usually limited to chemical applications [26, 45, 46] and modality-specific stimuli like heat and cold [25] or mechanical stress [34]. In our protocol, we employed local electrical stimulation with

an almost single-cell precision and bypassed the unselective applications of modality-specific assays. As a result, by selective application of stimulus trains, we intended to imitate the encoded sensory signals which may originate from any modality.

In a previous related study, Newberry et al. developed spontaneously active DRG cultures grown on MEA plates in order to study sensory neurons within a network context [26]. Afterwards, Black et al. conducted experiments with DRG neurons on multi-well MEA platforms and observed synchronous and correlated activity, which was discussed to be originating from gap junctions but not synaptic connections [25]. By using glutamatergic receptor antagonists, we successfully blocked the interconnected activity and showed the existence of glutamatergic post-synapses in cultured DRG neurons functionally. Subsequently, we investigated the presence of synapse formations structurally using ICC technique. Synapses were effectively stained with the pre-synapse marker synaptophysin. These successive findings, for the first time, confirmed the materialization of complete synapses and formation of synaptic networks in the DRG cultures.

The first part of our extracellular electrophysiology experiments defines the primary neuronal responses to stimulation and, the second part shows the basic interaction profiles between the primary and the secondary neurons. The third part investigates the network properties involving interactions of multiple neurons. Analyses summarized in Figure 2.6 shows the excitability alterations and thus the decreased thresholds of excitation. In addition, it is found that the number of connected pairs are also increased after repetitive stimulation. Significant changes occur due to repetitive stimulation and these findings suggest an underlying synaptic facilitation mechanism [40].

Causal transitions of the neuronal activity are not covered in this study and exact axonal tracing is left for future studies. Since the connections are essentially axonal, instead of only monitoring the neuron bodies, use of an axonal-GCaMP indicator could provide more information by allowing imaging of axonal calcium transitions [50]. Since dissociated cell culture models lack organizational structure and deviate from *in vivo* conditions, we recommend additional experiments involving explant or

slice cultures which would be more confluent with denser interactions.

We developed a versatile setup to study the network behavior of adult DRG neurons *in vitro*. This setup combines MEAs for stimulation and genetically encoded calcium indicator (GECI) based monitoring. The sensitivity achieved by Ca^{2+} imaging allows recording from adult DRG neurons *in vitro* without resorting to any inflammation model. Evoked responses from cultured DRG neurons through almost single-cell stimulations showed similarities between individual responses and correlation analyses verified statistical relationships between neurons. We demonstrated that this correlation originates from functional synaptic connections using glutamatergic post-synaptic blockers. Applying pre-synaptic marker synaptophysin, we verified the presence of synapses also structurally. Multi-layer network experiments revealed that continuous stimulation increases coupling strength of neurons. Our results suggest a new type of neuron-to-neuron interaction conducted through synaptic connections in cultured DRG neurons in which a stimulated neuron either modulates spontaneous activity of other neurons or activates previously quiet neurons.

Somata of sensory neurons do not form any synapses with each other inside the DRG *in vivo* [17, 51, 52, 53]. However, we have shown synapse formation between DRG neurons *in vitro*. In dissociated culture model, DRG neurons are released from ganglion structure and, connective and glial tissue layers are removed. This alteration can be a cue for synapse formation. In addition, the dissociation procedure itself may act as an injury model which is known to reprogram DRG neurons and temporarily alter cell identity [54, 55]. Functional and structural synapse formation and network development potential of sensory neurons may explain neuron-to-neuron interactions in a new scope [18]. These findings may shed new light on various disorders such as neuropathies, fibromyalgia, small fiber neuropathy, immune-mediated hyperalgesia, and other pain syndromes of peripheral nervous system [56, 57].

3. PLATFORM II: A NOVEL TOOL FOR CLOSED LOOP EXTRACELLULAR ELECTROPHYSIOLOGY - IMPLICATIONS FOR CULTURED NEURONAL NETWORKS

Cultured neuronal networks (CNNs) are excellent tools for studying how neuronal representation and adaptation arises in networks of controlled populations of neurons. To ensure interaction of a CNN and an artificial setting, reliable operation in both open and closed loop should be provided. We integrated optogenetic stimulation with microelectrode array (MEA) recordings through the use of a digital micro mirror device. We developed a 64-channel interface for neuronal network control and data acquisition. We determined the "best" light intensity, frequency and duty-cycle parameters for stimulation through trial-and-error. This resulted in robust and reproducible neuronal responses. We demonstrated both open and closed loop configurations in the new setup involving multiple bidirectional channels. Optogenetic stimulation removes the electrical artifacts and the limitation on the number of stimulation channels. In addition, the use of electrical recording provides continuous and high-precision temporal monitoring of electrical activity. Unlike previous approaches that combined optogenetic stimulation and MEA recordings, we did not use binary grid patterns, but assigned an adjustable size, non-binary optical spot to each electrode. This facilitates adaptation of the stimulation parameters. Through example applications we showed that this platform is highly reliable and can be especially useful in closed loop electrophysiological research. The presented platform is schematically summarized in Figure 3.1. It meets the requirements of research in neuronal plasticity, network encoding and representation, closed loop control of firing rate and synchronization. Moreover, it can also be very useful in developing adaptive stimulation strategies.

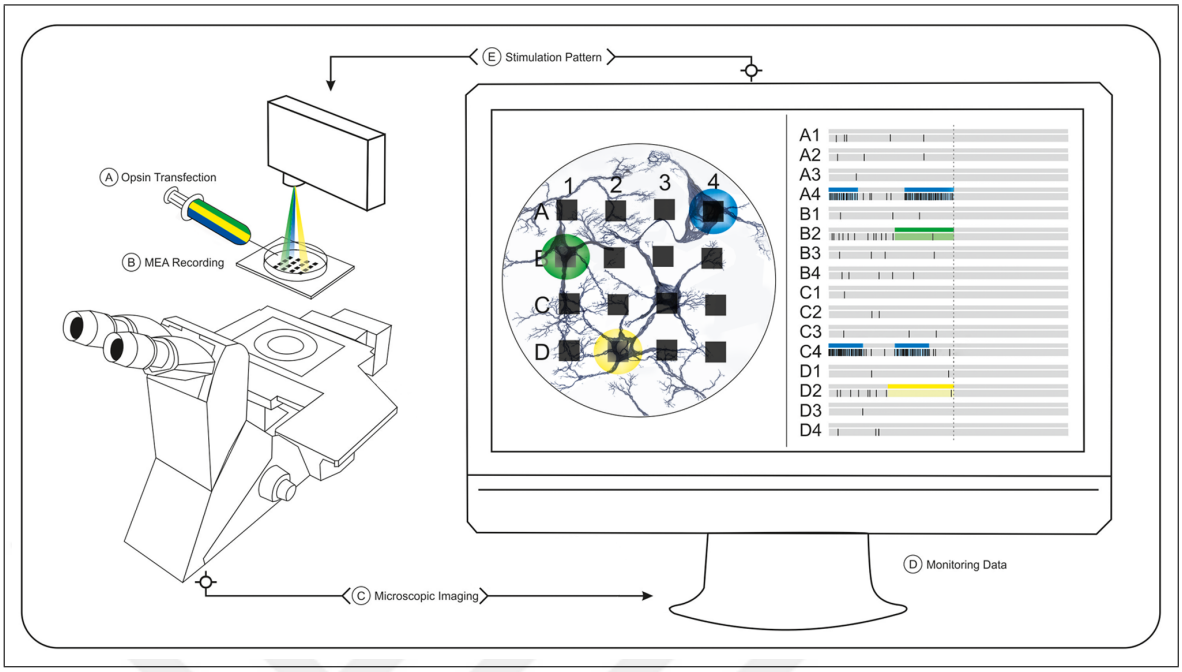

Figure 3.1 Capital letters represent some of the crucial components or procedures of the experimental platform II. (A) Opsin Transfection: Transduction of neurons with adeno-associated virus-mediated lightsensitive channel proteins. (B) MEA Recording: Extracellular action potentials being recorded from hippocampal cells cultured on Multi Electrode Array plates. (C) Microscopic Imaging: Observation of applied stimulation patterns with an inverted microscope. (D) Monitoring Data: Neuronal activity through 64 channels of the MEAs coupled to the data acquisition system. (E) Stimulation Pattern: Closing of the loop by application of designed stimulation patterns with the digital light processing projection system.

3.1 Introduction

Understanding how input signals are represented and output signals produced in a specified brain circuit is difficult because of the large number of participating neurons and their complex interactions. Extracellular electrophysiology is a valuable method for developing and designing artificial devices that communicate with large populations of living cells. To this end, both individual and population neural coding dynamics should be well defined, which requires the ability to conduct both bidirectional and closed-loop experiments. Commonly, electrical recording and electrical stimulation techniques are used together to meet these requirements. Electrical stimulation leads to inevitable stimulation artifacts that prevents recording from all the electrodes during stimulation. The artifacts can also saturate the recording circuitry and this increases the time lost to larger scales [58]. To avoid and correct artifacts, advanced modifications are neces-

sary both in hardware and software. However they do not fully remove the problem. An alternative to electrical recording for monitoring neuronal activity while applying electrical stimulation is calcium imaging, also known for its high spatial resolution. However, calcium imaging has very poor temporal resolution compared to electrical activity recordings [59]. Another solution is to replace electrical stimulation with optogenetic stimulation which provides temporally precise control of cellular activity and is devoid of the problems encountered in electrical stimulation. In addition, optogenetic stimulation tools (ChR2, NpHR, Arch) allow both excitation and inhibition of the cell by controlling various ion channels and pumps (Na^+, Cl^-, H^+). Therefore, the integration of optogenetic tools stands as an appealing technique for performing bidirectional assays, particularly involving cultured neuronal networks.

Although the limitations in bidirectional electrical interfaces can be overcome with optogenetics, closed loop setups have not yet been much improved and are restricted to only a few input-output channels. On the other hand, closed loop assays in cultured neuronal networks provide the most proper tools for investigating communication between a biological neuronal network and an interacting electronic device [60]. The development of closed loop platforms is important for studying neuronal encoding, representation, and adaptation as well as for the advancement of adaptive stimulation strategies. These phenomena can be better interrogated by inclusion of multiple input-output channels.

We integrated MEA based multi-channel electrical activity recording and spatiotemporally controlled optogenetic stimulation through a digital micro mirror (DMD) based spatial light modulation system. The DMD based optogenetic stimulation has had several previous implementations, including local and wide field illumination of the CNN. In addition, these implementations used both multiple extracellular and single intracellular recording channels. Among the works involving local stimulation and MEA recording, [61, 62] projected a binary grid pattern on the electrode area, which was conceptualized in [63]. Although the binary grid pattern approach covers all the recording electrodes, it does not provide perspective of multiple channel input/output (I/O) interfacing.

Our setup is the first implementation of MEA recording and DMD based optogenetic stimulation in a one-to-one mapping context. Considering optogenetic stimulation and electrical recording as input and output, we designed a 64-channel I/O interface specifically for cultured neuronal networks. In our design, we incorporated adjustable-size and non-binary spots for each input instead of using a binary grid pattern. Hence, our approach allows one to generate adaptive stimulation strategies which can be very useful in closed loop assays. Exclusion of the electrical stimulation artifacts removed the issues such as the common artifact reflected on all electrodes and the recovery time of the stimulation electrode as defined in [64]. Moreover, the use of optical stimulation eliminated the limitation in number of bidirectional channels, for electrical stimulation it is a drawback as reported in [65]. Consequently, our approach increases the reliability of closed-loop experiments since MEAs allow continuous and high-precision temporal monitoring of electrical activity.

I/O channels that can be used independently would improve studies on network encoding and representation especially in network level investigations that require multiple channels. Multiple accessing and probing feature of our approach would also enhance local analyses in toxicity screening assays [66]. Increased reliability in closed loop operation allows improved control of firing rate and synchronization. We believe that our setup will provide an ideal working environment for the development of adaptive stimulation strategies for prosthetic devices and pacemakers.

3.2 Materials and Methods

3.2.1 MEAs

Two types of multi-electrode array (MEA) plates, MMEP-4 and MMEP-4R, were used in the reported experiments which were both purchased from The Center for Network Neuroscience of the University of North Texas. The former, type MMEP-4 has a standard 8 by 8 matrix layouts with 150 μm equal spacing between electrode centers and 24 μm electrode diameters. The second, MMEP-4R has 64 electrodes

as well, within a condensed, pseudo-hexagonal layout. Each electrode has a 18 μm diameter and 70 μm equal spacing between each other, thus making a 0.28 mm^2 active area, which has a one fourth scale of the first type whose total active area is 1.15 mm^2. Layout and scale features of MMEP-4 and MMEP-4R are shown in Figure 3.2(c) and (d). Before use, polystyrene frames of 35 mm Petri dishes (Thermo-Fisher) were adhered to MEA plates using a biocompatible adhesive (Hollister-7730), a top view of a prepared MEA plate can be seen from Figure 3.2(a). Washed MEA plates with 10% bleach, 70% ethanol and double distilled water were then exposed to UV light for two hours for sterilization. After that, an appropriate coating was used to provide a primary extracellular matrix for cell adhesion. Sterilized MEA plates were exposed to a torch flame for a 0.5s duration in order to activate the surface insulation. Afterwards, 0.1% polyethylenimine (PEI, Sigma-3880) in 0.1M borate buffer and 1% Laminin (Sigma-L2020) in double distilled water solutions were coated by incubation of each one at 37°C overnight.

3.2.2 Culture Protocol

All animals were handled in strict accordance with guidelines for animal care and use issued by the European Community directive 86/609/CEE. All animal work was approved by *the Committee on Ethics of Animal Experimentation of Istanbul Medipol University* (IMUHADYEK). Transgenic mice strains which were originally obtained from The Jackson Laboratory (USA), kept and bred in experimental animal center of our institution. Utilized strains were Vgat-ires-cre (Stock: 016962) and Vglut2-ires-cre (Stock: 016963).

Postnatal day 0 to 4 Balb-c mice were used for dissociated hippocampal cultures. Rapid decapitation and dissection of the brains were performed in a sterile laminar flow hood. Isolated hippocampi were kept in L15 (Sigma-L5520) medium at 4°C with an addition of 10U papain (Sigma-P4762) enzyme for 45 minutes. After enzyme digestion, hippocampi were gently triturated with fire-polished Pasteur pipettes with decreasing diameters and transferred into a new L15-based medium including 10% FBS (Sigma-

F4135) for enzyme inactivation. Then by centrifuging at 900 rpm for 5 minutes at 4°C and eliminating the supernatant, final suspension including cells was obtained. The suspension was diluted with NBA (Gibco-A10888-022) medium containing 1% glutaMAX (Gibco-35050061), 1% Antibiotic-Antimycotic agent (Sigma-A5955), 2% B27 (Gibco-17504044), and 5% horse serum (Gibco-26050088) before plating. Hippocampal cells were seeded on pre-coated MEA plates with a confluency of 80-100%. To concentrate the desired number of cells onto the active areas of MEA plates, 10-20 thousand cells/mm^2, cloning cylinders (Sigma-C7983) were employed. The cultures were kept in an incubator at 37°C and 5% CO_2 thereafter and half of the medium was replenished in every four days. An excerpt of a typical hippocampal network grown on MEA surface is shown in Figure 3.2(b) at its fourth day *in vitro*.

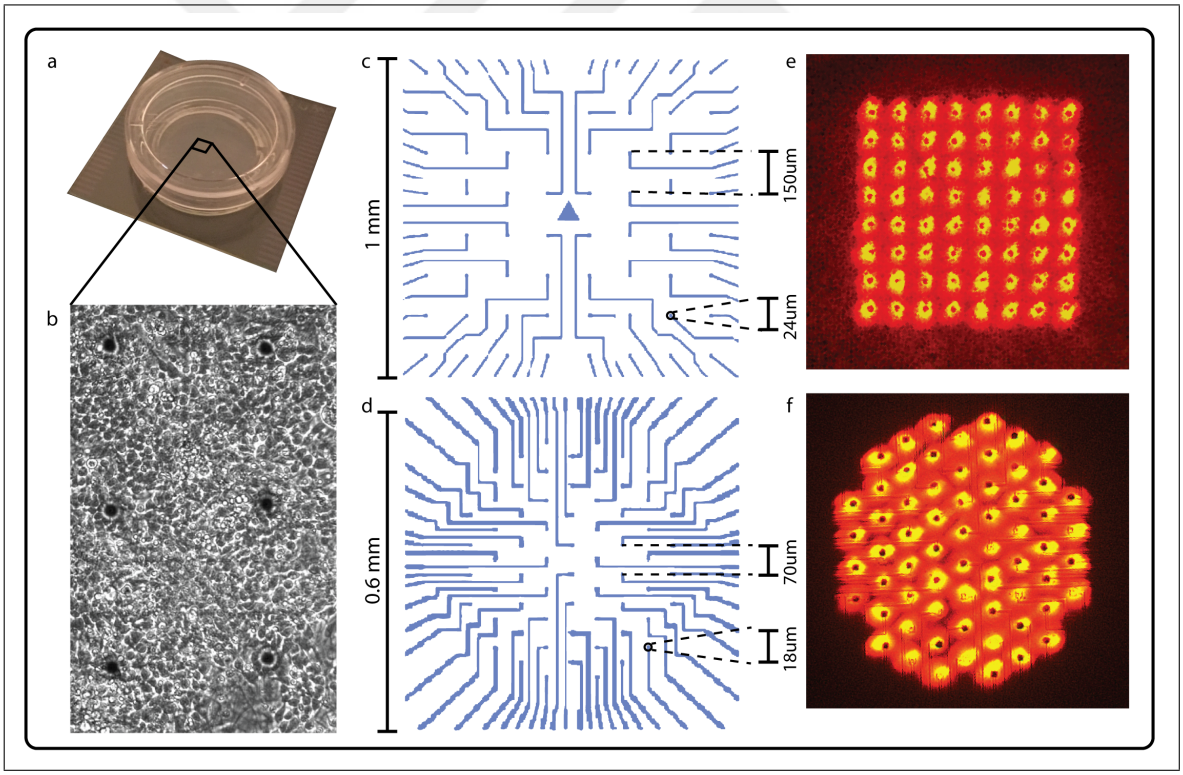

Figure 3.2 CNNs on MEA plates. (a) A 5×5cm MEA plate. (b) Location of the cells on the electrode surface DIV18. (c) and (d) Layout and scale features of MMEP-4 and MMEP-4R plates. Distances between electrodes are 150 and 70 μm for c and d. (e) and (f) Light spots circling the electrodes for calibration. 70 and 40 μm are averaging diameters of the light spots for e and f. Light spots were refracted through 1 mm thick glass and culture media.

3.2.3 Optogenetics

To make the cells express channelrhodopsin (ChR2), two types of home-produced viral vectors were utilized. The first one was the *rAAV-CAG-hChR2-H134R-tdTomato*, recombinant AAVs carrying H134R mutation of the ChR2, tagged with tdTomato, and controlled by the CAG promoter which resulted an efficient transfection rate on all cell types of our mixed hippocampal cultures. The second was the *rAAVEF1a-FLEX-hChR2(H134R)-mCherry*, a cre-dependent ChR2 vector, driven by EF1a promoter and fused with mCherry. Cre-dependent plasmids function only in the cells expressing cre recombinase expressing cells, hence when applied to the cultures prepared from cre animals, selective ChR2 expression was achieved. A ChR2 transfected hippocampal culture from a vGlut-cre mouse, can be seen from Figure 3.3, left box at the middle expressing mCherry fluorescent. The transgenic mice strain was purchased from Jackson Laboratories, a knock-in strain, Vglut2-ires-cre (C57BL/6J), having Crerecombinase enzyme expression only in glutamatergic neurons. By trial-and-error, it was determined that application of the viral vectors after four or five days *in vitro* yielded the highest rate of transfection. Fluorescent microscopy was used for checking the expression of the ChR2s, which were marked with tdTomato and mCherry. Expression took on an average of four or five days as well to reach an adequate level for experimental use.

3.2.4 Electrical Recording

MEAs having 32 contact pads at its right and left sides were coupled to Plexon (MHP64) headstage via two zebra strips and the headstage was linked to Plexon 64 channel analog preamp which had 1000× gain with a band pass filter of 0.7-8000 Hz. Preamp output was interfaced with two identical and interconnected 32-channel data acquisition boards (NI-PCIe-6353) installed on a Lenovo PC. Figure 3.4, bottom path, from left to right, represents the switching from analog to digital. The signals were acquired at 20 kHz for monitoring sessions and at 10 kHz for closed-loop assays where spike detection run simultaneously. All data monitoring and signal processing

issues were accomplished using custom written Matlab (Mathworks Inc.) codes which utilized the Data Acquisition Toolbox (Mathworks Inc.) and National Instruments (NI) libraries. An adaptive thresholding approach was used for spike detection, which was adapted from a previous study [67]. Adaptiveness was achieved by carrying out the computation in moving time windows to overcome unintended variations in noise levels. In addition, to remove artifacts that were detected together with the spikes a template matching process adapted [68], since the artifacts did not have the spike waveform features [69].

3.2.5 Software

Design of optical stimulation patterns were achieved with a slave PC (Lenovo) which controlled the digital light processing (DLP) projection system. Data communication between master and slave PC was performed with user datagram protocol (UDP) via Ethernet. All stimulation-related processes were handled by custom written Matlab codes. In the dashed-line rectangle box at the right part of Figure 3.3, possible function modes are shown. First mode is the calibration mode which includes adjustment specifications and design parameters. Figure 3.2 (e) and (f) show calibration images where all channels were selected with an arbitrary wavelength and intensity, but positioned spots with specified diameters. Second and third paths in the box represent open and closed loop operation choices, respectively. In the open-loop section, one can determine any stimulation pattern to be applied periodically and record electrical activity in any desired time. Feedback parameters or event-flags were expected for initializing both the stimulation and the recording, when the closed-loop mode was selected. Stimulation parameters as well as light patterns can be designed adaptively alterable in response to streaming feedback data. Typical feedback parameters employed in the experiments were firing rate, spike coincidence and synchronization index.

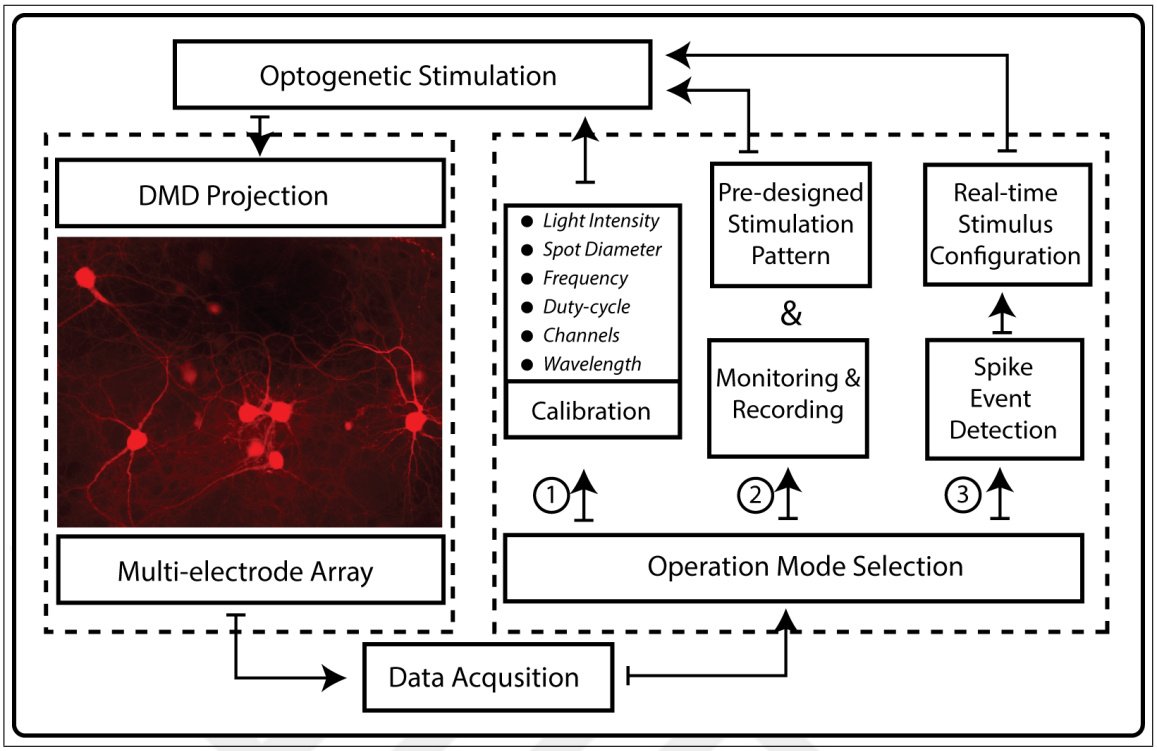

Figure 3.3 Flow diagram. Dashed rectangle at left and right portions of the diagram indicate wetware and software parts, since the blocks on upper and lower sections show interface units. (1), (2), and (3) shown with arrows and paths are the system function options. First is the calibration mode which includes adjustment specs and design parameters. Second and third are open and closed loop operation modes.

3.2.6 DLP Stimulation Setup

A Lightcrafter-4500 DLP projector development kit (Texas Instruments), having a resolution of 1280x800 diamond pixels and RGB led sources (OSRAM-Q9WP) that were driven by digital micro mirror devices (DMDs), was incorporated as the stimulation interface. An invert microscope (Olympus-CKX41) was dedicated for simultaneous verification of the spatial accuracy of stimulation as well as for calibrating the focal distance. By dismounting the bright field lighting attachment of the microscope and substituting the DLP projector instead, a height adjustable mechanism was attained for the projection system. Top part of Figure 3.3 shows the return path to the wetware, the DMD interface redirecting the designed light patterns.

3.3 Results

Healthy populations of hippocampal cells, cultured on MEAs, developed spontaneously active neuronal networks. Prior to experiments, we imaged ChR2 expression rates in these hippocampal networks under fluorescence microscopy. A ChR2 expressing network grown on MEA at DIV35 is shown in Figure 3.6(a), where both neurons and glial cells are marked with tdTomato.

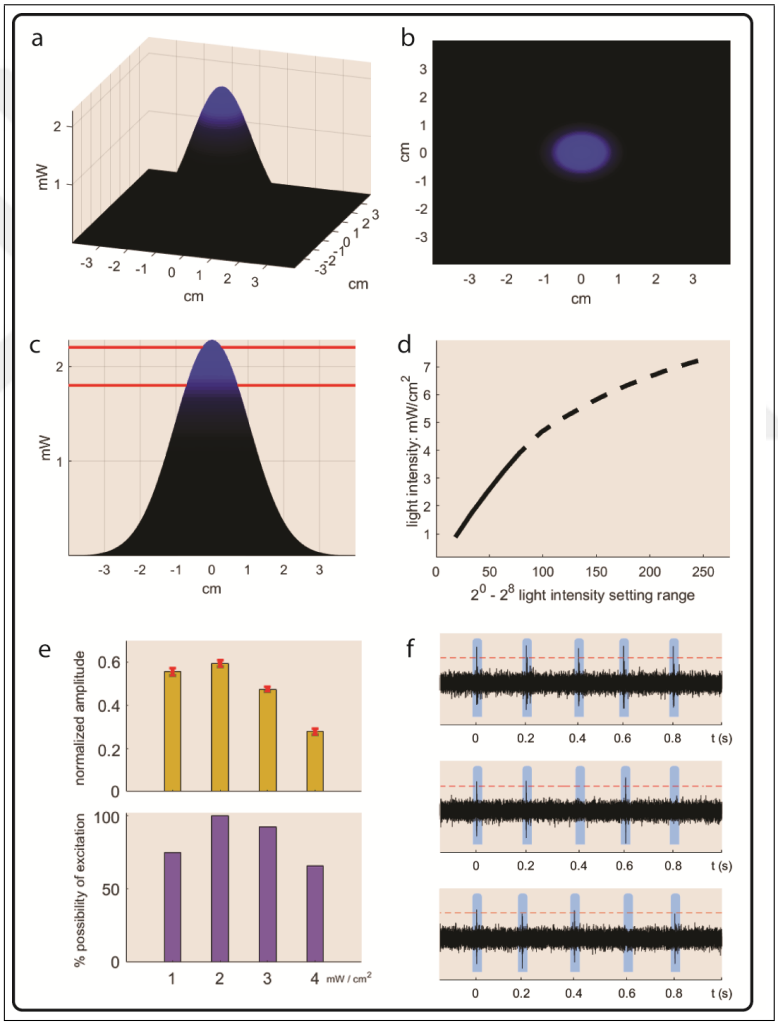

Figure 3.4 Intensity. (a) Gaussian profile of light intensity in mW/cm^2, measured at 470nm (b) and (c) Top and side views. Effective section shown between red lines. (d) Light intensity adjustment scale. Line and dashed-line indicate sufficient and excess ranges. (e) Response profiles under four light intensity values: 1, 2, 3 and 4 mW/cm^2. Mustard colored bars represent normalized response amplitudes. Purple bars represent respond possibility of stimulated cells. (f) Characteristic responses summarized in (e). Typical time series shown in (f). Responses to 2, 1, and 3 mW/cm^2 light intensity stimulations are shown in top, middle and bottom rows respectively.

3.3.1 Light Intensity

In majority of our stimulation scenarios, circular light spots of 488 nm were used. Light intensity and its distribution was modelled using measurements which exhibited Gaussian profiles. Measurements conducted with an optical power meter (Thorlabs Inc. PM130D) having a 470 nm built-in photodiode, which provides light intensity reads in milliwatts per square centimeters. Figure 3.4(a) illustrates the 3d Gaussian curve produced by the model and Figure 3.4(b) represents a top view projection. To stimulate both the neurons located on and in the vicinity of a recording electrode, light spots were created two or three times wider than the electrode area. Utilized light intensity range in the experiments was marked on the Gaussian curve with red lines in Figure 3.4(c). Figure 3.4(d) shows the curve obtained from the measured light intensity values which correspond to the operating range of LED light sources. Solid and dashed parts of the curve show linear and saturated ranges respectively.

Effective range of light intensity for stimulation varies among incorporated light sources or optical pathways as well as ChR2 type, transfection efficacy and expression rates [70]. To obtain successful and repeatable neuronal responses in our setting, we determined effective range as, 1-4 mW/cm^2, which coincides with the linear part of the curve shown in Figure 3.4(d). In actual experiments, the circular light spots that we used for stimulation had radii between 10-40 μm, which correspond to spot areas less than 5000 μm^2 (0.005 mm^2). In addition, the light passes through cell culture medium and polystyrene cap of the Petri dish and this produces unintended dispersion and refraction. As a result, light intensity levels which were adjusted according to the calculations based on theoretical and measured results do not reflect the real light intensity dose to the neurons. Characteristic evoked responses to 1-4 mW/cm^2 stimulation are summarized in Figure 3.4(e). Below and above the optimal value, both the possibility of evoking neuronal responses and the amplitude of the produced action potentials decrease. Figure 3.4(f) illustrates these optimal, decreased possibility and decreased amplitude cases in top, middle and bottom rows, respectively.

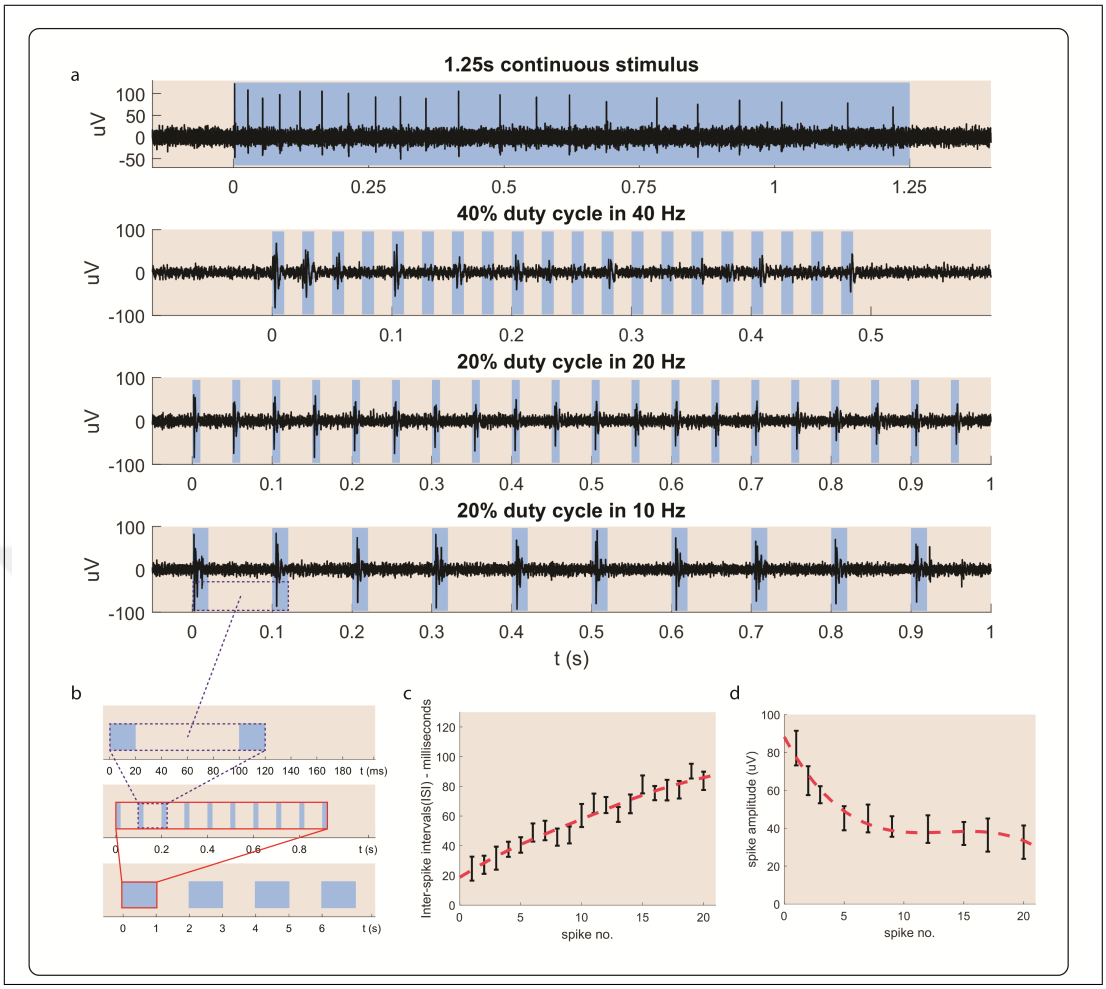

Figure 3.5 Determination of optimal stimulation frequency and duty cycle. (a) Four examples of frequency and duty-cycle optimization. From top to bottom, (i) to (iv). (i) continuous stimulation of 1.25s duration (ii) 25 ms period, 10 ms stim duration, packed in total 0.5 s with 20 pulses (iii) 50 ms period, 10 ms stim duration packed in total 1s with 20 pulses (iv) 100 ms period 20 ms stim duration packed in total 1s with 10 pulses (b) Stimulation pulse packets (c) Inter-spike intervals increase in continuous stimulation case. (d) Spike amplitudes decrease in high frequency and high duty cycles similar to the continuous stimulation case.

3.3.2 Frequency and Duty Cycle

We looked for optimal duration and frequency of stimulation pulses to evoke reproducible neuronal responses following every stimulation pulse. When a continuous stimulation pulse was considered for a limited period of time, responsiveness of the neurons to the stimuli decreased. First row of the Figure 3.5(a) demonstrates the neuronal responses to a continuous stimulation of 1.25 s. Rate of spike occurrence and spike amplitudes decrease gradually, as can be seen from Figure 3.5 (c) and (d) respectively. Since the emerged decrease was unintended, we explored temporally spaced

configurations of light pulses. We fixed the length of an individual stimulation epoch at one second which comprised of pulses and spaces. Duration of individual light pulses in a stimulation epoch chosen as 10 or 20 milliseconds similar to a previous work [71]. Frequency of these pulses and their duty cycle were determined within the range of the kinetic limitations of ChR2 [72]. Second to fourth rows of Figure 3.5(a) shows optimization steps of these parameters, where the last row is the final configuration. Epochs typically applied within 1s on and 1s off times as were given in Figure 3.5(b).

3.3.3 Experimental Procedures

We determined sites of cells or cell assemblies where stimulation induces neuronal activity and electrodes that allow recording of this activity. We defined these sites and electrodes as ready-to-use input/output channels, considering that a channel can be constituted by one or more recording electrodes. To carry out the above procedure, area scanning stimulation is applied while multi-channel electrical activity is monitored and recorded simultaneously. A typical electrical activity recording, performed through a scanning stimulation, is shown in Figure 3.6(b). In this instance, neurons in the vicinity of all 64 electrodes are stimulated in sequence with 100 ms pulse duration allocated for each. This sequential stimulation was repeated in 10s periods and post stimulus time histograms (PSTH, bin width 40 ms) were created. Then, averaged PSTHs were sorted depending on their stimulus-specific prominence as shown in Figure 3.6(c).

3.3.4 Closing the Loop

Typical feedback parameters employed in the experiments were synchronization, firing rate and spike coincidence. Synchronization indicates whether the activity mode of the network is synchronized within a defined period or not, and it is calculated in defined time intervals as shown in a previous study [73]. Firing rate can be computed using a time bin of a specified duration, counting the number of spikes detected per

time bin. When a pre-defined threshold for rate is exceeded, a flag will be triggered to activate a fixed or an adaptive stimulation pattern. Coincidence of a number of spike events detected from selected channels in a time interval provide also a flag, similar to the firing rate trigger.

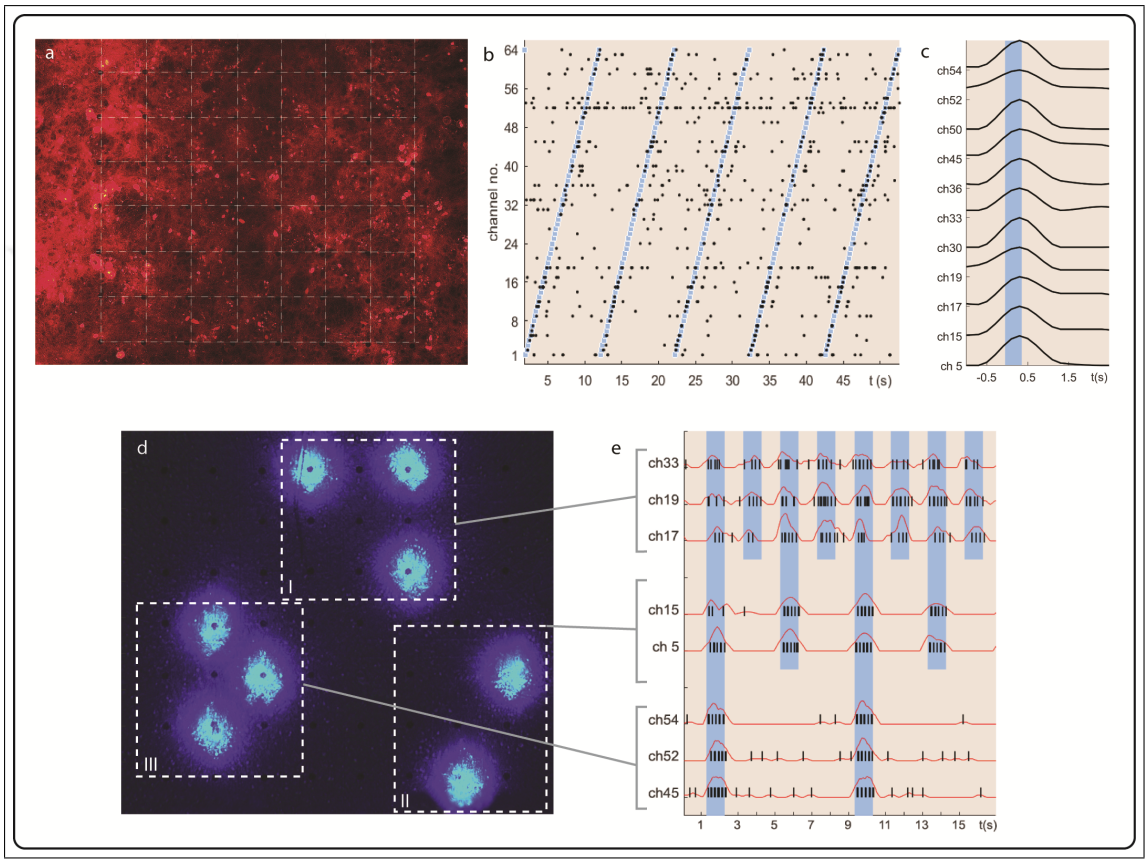

Figure 3.6 (a) Channel-rhodopsin expressing cells expressing tdTomato fluorescent. Dashed grid in white shows electrode positions at intersection points. (b) Scanning stimulation of 64 electrodes and neuronal responses. A synfire chain like task. (c) Post-Stimulus-Time-Histogram (PSTH) of selected channels which respond consistently. (d) Three groups assigned for poly-rhythmic stimulation shown in a bright field image. Black dots are electrodes and blue spots are stimulation light pulses. (e) Recorded responses of the three groups exhibit three distinct spike rates.

The first feedback parameter incorporated is the synchronization index (vector strength) that indicates instances of synchrony [74]. To illustrate this, a controlled synchronization application is shown in Figure 3.6 (d) and (e). In this application the network is separated into three zones, and different stimulation frequencies are applied on these zones. The second feedback option utilizes rate detection, which is based on the counting of the detected spikes within a definite time window. If the frequency of

the spike events exceeds a chosen threshold value, a stimulation signal will be directed to a defined site in the network. A typical application is introduced in Figure 3.7(a), where the red spot indicates the measurement site and the blue spot indicates the stimulated site. Blue arrowheads marked on time series, previously defined as flags, indicate exceedance of the threshold (selected as three spikes per bin). Upper time series zooms in a 100 ms time bin where three spikes were counted. The third feedback approach involves the detection of coincident firing of two neurons from two different locations (red spots in Figure 3.7(b), A and B). If the coincidence is detected within a 10 ms time bin, a third site in the network gets stimulation signal (blue spot, C). Two typical coincident events indicated with blue flags are shown, where the sequence of spikes alternate.

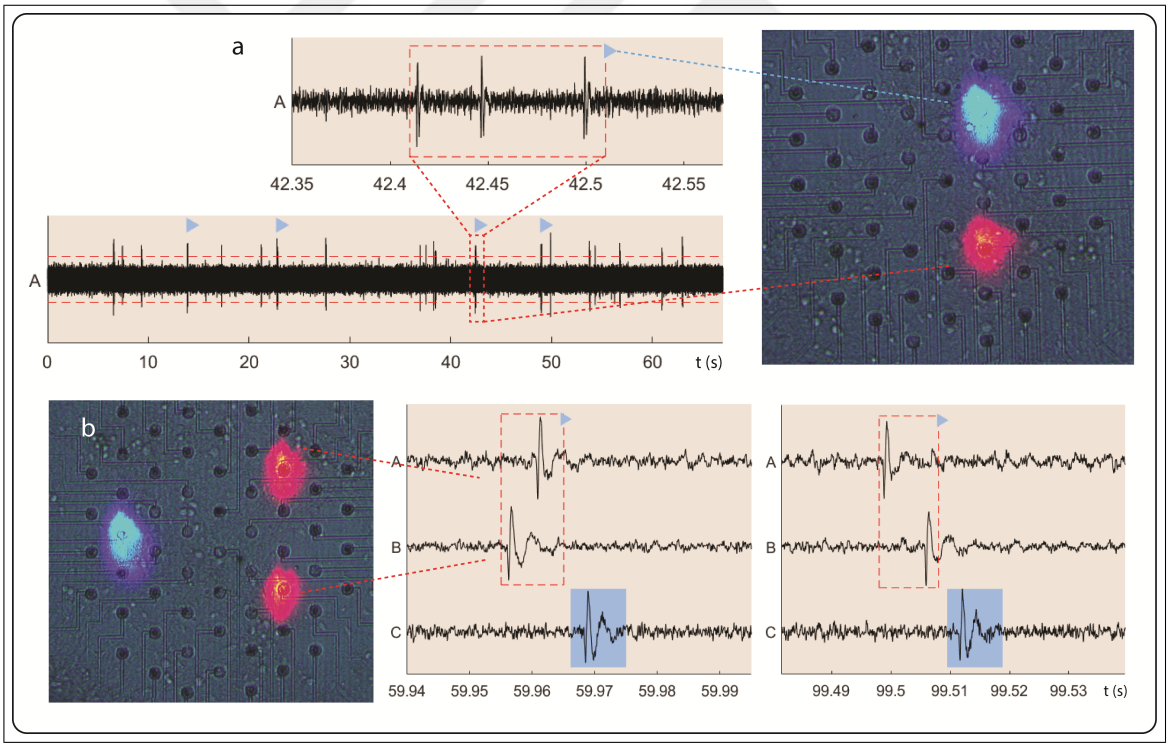

Figure 3.7 Feedback. Red and blue spots indicate the locations of event-detection and stimulation locations respectively. Blue arrowheads represent system flags. Dashed-line rectangles in red indicate detected events. Rate detection: Spikes detected in 100 ms bins. If more than two, an arbitrary threshold, spikes detected in the 100 ms intervals, it is assumed that the spike rate is increased. In response to that increase, system sets a flag, and actuates the stimulator. Coincidence detection: Spikes from two channels detected. If two spikes detected from two channels, within 10 ms intervals, it is assumed that a coincident event is detected. In response to that coincidence, system sets a flag, and actuates the stimulator.

3.4 Discussion

To interface cultured neuronal networks with multiple input-output channels, we developed a practical and versatile experimental setup. We emphasize cultured neuronal networks. However any kind of electrogenic cell can be grown on MEAs and used in our setup. More specifically, we studied hippocampal networks of only neurons or only excitatory neurons expressing ChR2. Likewise, the flexibility in cell type, cellular specificity can be altered by genetic targeting methods. Instead of using generic target proteins that are shared by many cell types, only the cell type of interest can be targeted [75]. Besides, individual cells may express both excitatory and inhibitory optogenetic channels that can be controlled with different wavelengths [76]. Since the use of optical stimulation allows one to produce spatiotemporally controlled light patterns with adjustable wavelength compositions, various optogenetic tools can be used in appropriate combinations.

Integration of optogenetic stimulation to electrical recording platforms has been carried out in various approaches and combinations. For electrical recording, both intracellular and extracellular recording techniques are employed. All given studies in Table 3.1 except [77] and [78] resort to multi-channel extracellular recording approaches involving MEAs since they provide manipulation of and access to multiple nodes of a network. These exclude studies involve patch clamp, which achieves exact spatial resolution but trades off the multiple channel operation.

The techniques used for optogenetic stimulation include a variety of options because the alternatives that make up the optical system are numerous, and experiments require flexible designs. The light source can be LEDs or lasers that need to be processed later for focusing or de-magnification. Wide field illumination of the sample, in which the light is directly projected onto the whole network area is the most preferred application since it does not need further processing [79, 80]. Typical methods for focusing patterns of light onto cellular scales are integration into the ready-made optical path of the microscope [78, 81, 61, 82, 62, 83], fabrication of micro-LED arrays [77], and design of specific waveguides [84]. To generate localized light patterns, scanning

laser switching [82], liquid crystal (LC) [81, 61, 83], and digital micro mirror (DMD) [78, 62, 85] based spatial light modulation techniques are the most preferred options.

Table 3.1
Electrical recording used with optogenetic stimulation.

	Optical system	**Electrical recording**	**Stimulation area**
Ref. [85]	DMD	MEA	Local (Binary grid)
Ref. [61]	LC-SLM (through microscope)	MEA	Local (Binary grid)
Ref. [80]	LED	MEA	Wide field
Ref. [77]	OLED Microarray	Patch Clamp	Local
Ref. [84]	Laser (through waveguide)	MEA	Local
Ref. [78]	DMD (through microscope)	Patch Clamp	Local
Ref. [82]	Switched Laser (through microscope)	MEA	Local (scanning)
Ref. [83]	LC-SLM (through microscope)	MEA	Local (holographic)
Ref. [81]	LC-SLM (through microscope)	MEA	Local (masking)
Ref. [79]	Power LED	MEA	Wide field
Ref. [62]	DMD (through microscope)	MEA	Local (Binary grid)
Present work	DMD	MEA	Local (adaptive)

Bidirectional and closed-loop terms are frequently used for defining bilateral operation including activity monitoring and manipulation of electrogenic tissue, although bidirectional can be achieved both in open- and closed-loop. Recording the activity while applying stimulation is sufficient for open-loop operation. However for closing the loop, at least a stimulation parameter should be determined depending on a mea-

sured quantity of the ongoing activity. Some important studies that have been carried out meeting this requirement are listed in Table 3.2. The first study in Table 3.2 uses single channel local electrical stimulation and 64 channel electrical reading [86]. They compute the ratio of average network response to stimulation as the control parameter which is fed back in 20s time intervals. This feedback is compared to a threshold and stimulation is applied with an on-off control approach. Stimulation artifact due to electrical stimulation causes 20 ms time loss after stimulation; this can be compared with previous applications. The remaining studies use 59 channels of MEA recording and whole-field optical stimulation [79, 87]. They incorporate average firing rate as the feedback parameter updated in 4-10 ms time bins. The stimulation strategy of these works involves on-off, look-up-table, proportional plus integral control techniques.

Table 3.2
Closed-loop assays.

	Input channels	**Output channels**	**Feedback parameter**
Ref. [86]	Single channel electrical stimulation	64 channel MEA	Response to stimulation ratio
Ref. [87]	Whole field optogenetic stimulation	59 channel MEA	Total firing rate
Ref. [79]	Whole field optogenetic stimulation	59 channel MEA	Normalized firing rate
Present work	Local optogenetic stimulation	64 channel MEA	Local firing rate Coincident events Synchronization index

3.4.1 Implications for Cultured Neuronal Networks

To utilize optogenetic stimulation effectively, we determined optimal parameters (light intensity, duration of and interval between the light pulses) that yield reproducible and robust responses. Using channels bidirectionally and independently without the mentioned setbacks [88], we attained a reliable closed-loop experimentation platform. We demonstrated both open and closed loop modes of operation by exploratory applications involving multiple channels. A sequential spatiotemporal stimulation pattern in open loop (Figure 3.6(b)), performs as a network scanning or diagnosing tool, for determining network features. Identification of hub nodes using network features can be useful for finding effective stimulation sites [89, 90]. As a transition step between open and closed loop, which involves a synchronization index, separates the network into three groups spatiotemporally (Figure 3.6 (d) and (e)). With this controlled synchronization approach the network activity is partitioned and a kind of desynchronization is achieved instead of applying a randomized stimulation pattern [91]. Further studies relying on this approach can investigate inducing functional subclusters in a neuronal network.

Firing rate is the most conventional network parameter that is incorporated in closed loop applications [79, 86, 87]. In our example (Figure 3.7(a)) we utilized firing rate to artificially communicate two distinct nodes of the network in closed loop. We provided a more elaborate and advanced closed loop approach employing spike-event coincidence in Figure 3.7(b), which carried out an artificial communication as well. If spikes from two selected nodes were detected concurrently within a 10 ms time interval, a third node was stimulated. This approach can be used in spike timing dependent plasticity (STDP) and neuronal representation experiments where spike coincidence is critical [92]. In addition, in coincidence scenarios, occurance order of spiking events correspond to potentiation and depression [93]. In further studies, excitatory or inhibitory stimulations can be used in order of priority in accordance with the STDP concept.

3.4.2 Concluding Remarks

We presented a novel *in vitro* setup that integrates optogenetic stimulation and MEA recordings which we have considered as input and output to a CNN. By implementing adjustable-size and non-binary stimulation sites using a DMD, we realized artifact-free use of separate input-output channels. We believe that our approach will advance research on neuronal networks, particularly on adaptation and plasticity. Researchers who develop closed loop control techniques and adaptive stimulation strategies for network activity will benefit much from the new setup.

4. CONCLUSION

In this work, we studied cultured neural networks through their behavior and activity patterns. We used multi electrode arrays to capture electrical activity as well as to deliver electrical stimulation. On MEAs, we successfully grew healthy CNS and PNS cultures, observed network development in both. Additionally, we utilized optogenetic methods for activity monitoring as well as optical stimulation via light-activated channels.

In the context of activity monitoring, we examined extracellular action potentials obtained through MEA recordings. Also by using a genetically encoded Ca^{2+} indicator, GCaMP, we captured Ca^{2+} transitions utilizing fluorescent microscopy. To perform stimulation, we applied both electrical and optical techniques, employing MEAs and optogenetic approaches respectively. For achieving optical stimulation, we adopted a DMD based approach, which allowed projection of localized light patterns. We utilized ChR2, a cation channel that is activated by blue light, for optogenetic stimulation and determined working parameters for reproducible evoked neuronal responses.

To observe network formation thoroughly, we chose a spontaneously silent neuron type, DRG neurons, to solely engage in stimulated activities. For this purpose, we employed our platform, which combines electrical stimulation and calcium imaging. By applying biphasic stimulation to neuron somata adjacent to electrodes, we were able to quantify direct and secondary calcium transition patterns. Considering the indirect activity emerge as a result of synaptic connections, we also delivered the same stimuli with synaptic blockers present. Our analyses confirmed the synaptic connections as well as the network features which were altered after stimulation. Furthermore, by using immunocytochemistry, we showed localization of the synapses. Beyond that, this was the first study to demonstrate that DRG neurons had the ability to establish synaptic connections and networks.

Afterwards, we developed a pioneering platform that integrated local optogenetic stimulation to MEA recording instrumentation. This platform employs 64-channel micro electrode recordings and optical stimulation of each channel by assigned light spots, one-to-one coupled to each electrode. By integrating MEA recording setup with optical stimulation within a on-to-one coupling perspective, we had a versatile multi channel interface. We highlighted some of the potential applications that required bidirectional and closed-loop techniques in extracellular electrophysiology. Although a wide range of electrogenic cells could be studied in this platform, we specifically focused on CNNs and provided implications for ongoing research on CNNs.

We believe the techniques and platforms we used and developed can be useful in related areas of research. In addition to potential upgrades and refinements to current methodologies, we also anticipate future translational reflections.

APPENDIX A. Solutions and Media

Dissection Medium: Roswell Park Memorial Institute, (RPMI, Sigma) medium with addition of 1mM GlutaMAX-I (Gibco) supplement and 1% antibiotic-antimycotic solution which contains 100 U penicillin, 100 mg streptomycin and 250 ng/mL amphotericin-B (Sigma).

Culture Medium: Used for both culturing and maintenance stages of the cell culture, which consists of Neurobasal-A (NBA, Gibco) medium supplemented with 2% B27 (Gibco), 2 mM GlutaMAX-I (Gibco) and 1% antibiotic-antimycotic solution (Sigma).

Enzyme Solution 1: 100 U/mL collagenase (Sigma) enzyme added to the culture medium.

Enzyme Solution 2: 1 mg/mL trypsin solution (Sigma) and 50 μg/mL DNase (Sigma) enzyme added to the culture medium.

Enzyme Inhibition Medium: Culture medium including 700 μg/mL trypsin inhibitor (Sigma) and 10% fetal bovine serum (FBS, Sigma).

Gradient Preparation: Percoll, (Sigma) density gradient medium, was diluted at 10, 35 and 60% concentrations in culture medium in order to prepare a three-layer neuron purification-gradient, where neurons mainly aggregate at the middle layer after centrifuge.

Antagonists: NMDA antagonist AP5 (Sigma) and AMPA-Kainate antagonist CNQX (Sigma) were used 100 μM and 10 μM respectively and incubated in 37°C, 5% CO_2 incubator for 30 minutes to 1 hour prior to the experiments.

ICC Solutions: 3% bovine serum albumin (BSA, Sigma), 1% goat serum (Sigma) and 0.3% sodium azide (Sigma) diluted in phosphate buffer saline (PBS, Sigma) and 3% BSA, 1% goat serum and 0.1% Triton-X (Sigma) diluted in PBS were used as the blocking and the dilution solutions, respectively.

APPENDIX B. List of publications produced from the thesis

1. F. K. Bayat, B. Polat Budak, E. N. Yiğit, G. Öztürk, H. Ö. Gülçür, A. Güveniş, "Adult mouse dorsal root ganglia neurons form aberrant glutamatergic connections in dissociated cultures" *PLoS One. 2021 Mar 3;16(3):e0246924. doi: 10.1371/journal.pone.0246924.*

REFERENCES

1. Valdivia, P., M. Martin, W. R. LeFew, J. Ross, K. A. Houck, and T. J. Shafer, "Multi-well microelectrode array recordings detect neuroactivity of toxcast compounds," *NeuroToxicology*, Vol. 44, pp. 204–217, 2014.

2. Bradley, J. A., H. Luithardt, M. R. Metea, and C. Strock, "In vitro screening for seizure liability using microelectrode array technology," *Toxicological Sciences*, Vol. 163, pp. 240–253, 2018.

3. Cozzi, L., P. D'Angelo, M. Chiappalone, A. Ide, A. Novellino, S. Martinoia, and V. Sanguineti, "Coding and decoding of information in a bi-directional neural interface," *Neurocomputing*, Vol. 65-66, pp. 783–792, 2005.

4. Kermany, E., A. Gal, V. Lyakhov, R. Meir, S. Marom, and D. Eytan, "Tradeoffs and constraints on neural representation in networks of cortical neurons," *The Journal of Neuroscience*, Vol. 30, pp. 9588 – 9596, 2010.

5. le Feber, J., I. Stoyanova, and M. Chiappalone, "Connectivity, excitability and activity patterns in neuronal networks.," *Physical biology*, Vol. 11 3, p. 036005, 2014.

6. Charlesworth, P., E. Cotterill, A. Morton, S. Grant, and S. Eglen, "Quantitative differences in developmental profiles of spontaneous activity in cortical and hippocampal cultures," *Neural Development*, Vol. 10, 2014.

7. Ma, C., K. Greenquist, and R. LaMotte, "Inflammatory mediators enhance the excitability of chronically compressed dorsal root ganglion neurons.," *Journal of neurophysiology*, Vol. 95 4, pp. 2098–107, 2006.

8. Potter, S. M., "Chapter 4 distributed processing in cultured neuronal networks," in *Advances in Neural Population Coding*, Vol. 130 of *Progress in Brain Research*, pp. 49–62, Elsevier, 2001.

9. Fejtl, M., A. Stett, W. Nisch, K. Boven, and A. Möller, "On micro-electrode array revival: Its development, sophistication of recording, and stimulation," 2006.

10. Kandori, H., "Ion-pumping microbial rhodopsins," *Frontiers in Molecular Biosciences*, Vol. 2, p. 52, 2015.

11. Govorunova, E., O. Sineshchekov, H. Li, and J. Spudich, "Microbial rhodopsins: Diversity, mechanisms, and optogenetic applications.," *Annual review of biochemistry*, Vol. 86, pp. 845–872, 2017.

12. Chang, W.-P., J.-S. Wu, C.-M. Lee, B. A. Vogt, and B.-C. Shyu, "Spatiotemporal organization and thalamic modulation of seizures in the mouse medial thalamic-anterior cingulate slice," *Epilepsia*, Vol. 52, no. 12, pp. 2344–2355.

13. Roome, C. J., and B. Kuhn, "Simultaneous dendritic voltage and calcium imaging and somatic recording from purkinje neurons in awake mice," *Nature Communications*, Vol. 9, 2018.

14. Pienaar, I. S., D. T. Dexter, and V. Gradinaru, "Chapter 11 - neurophysiological and optogenetic assessment of brain networks involved in motor control," in *Movement Disorders (Second Edition)* (LeDoux, M. S., ed.), pp. 187–199, Boston: Academic Press, second edition ed., 2015.

15. Tung, J. K., K. Berglund, and R. Gross, "Optogenetic approaches for controlling seizure activity," *Brain Stimulation*, Vol. 9, pp. 801–810, 2016.

16. Krames, E. S., "The dorsal root ganglion in chronic pain and as a target for neuromodulation: A review," *Neuromodulation: Technology at the Neural Interface*, Vol. 18, no. 1, pp. 24–32, 2015.

17. Amir, R., and M. Devor, "Electrical excitability of the soma of sensory neurons is required for spike invasion of the soma, but not for through-conduction," *Biophysical Journal*, Vol. 84, no. 4, pp. 2181 – 2191, 2003.

18. Devor, M., "Unexplained peculiarities of the dorsal root ganglion," *Pain*, Vol. 82, pp. 27–35, 1999.

19. Monkhouse, S., *Cranial nerves: functional anatomy*, Cambridge: Cambridge University Press, 2006.

20. Ma, C., and R. H. LaMotte, "Multiple sites for generation of ectopic spontaneous activity in neurons of the chronically compressed dorsal root ganglion," *Journal of Neuroscience*, Vol. 27, no. 51, pp. 14059–14068, 2007.

21. Miller, K. E., E. M. Hoffman, M. Sutharshan, and R. Schechter, "Glutamate pharmacology and metabolism in peripheral primary afferents: Physiological and pathophysiological mechanisms," *Pharmacology and Therapeutics*, Vol. 130, no. 3, pp. 283–309, 2011.

22. Killian, N. J., V. N. Vernekar, S. M. Potter, and J. Vukasinovic, "A device for long-term perfusion, imaging, and electrical interfacing of brain tissue in vitro," *Frontiers in Neuroscience*, Vol. 10, p. 135, 2016.

23. Obien, M. E. J., K. Deligkaris, T. Bullmann, D. J. Bakkum, and U. Frey, "Revealing neuronal function through microelectrode array recordings," *Frontiers in Neuroscience*, Vol. 8, p. 423, 2015.

24. Vassallo, A., M. Chiappalone, R. De Camargos Lopes, B. Scelfo, A. Novellino, E. Defranchi, T. Palosaari, T. Weisschu, T. Ramirez, S. Martinoia, A. F. M. Johnstone, C. M. Mack, R. Landsiedel, M. Whelan, A. Bal-Price, and T. J. Shafer, "A multi-laboratory evaluation of microelectrode array-based measurements of neural network activity for acute neurotoxicity testing," *NeuroToxicology*, Vol. 60, pp. 280–292, 2017.

25. Black, B. J., R. Atmaramani, R. Kumaraju, S. Plagens, M. Romero-Ortega, G. Dussor, T. J. Price, Z. T. Campbell, and J. J. Pancrazio, "Adult mouse sensory neurons on microelectrode arrays exhibit increased spontaneous and stimulus-evoked activity in the presence of interleukin-6," *Journal of Neurophysiology*, Vol. 120, no. 3, pp. 1374–1385, 2018.

26. Newberry, K., S. Wang, N. Hoque, L. Kiss, M. K. Ahlijanian, J. Herrington, and J. D. Graef, "Development of a spontaneously active dorsal root ganglia assay using multiwell multielectrode arrays," *Journal of Neurophysiology*, Vol. 115, no. 6, pp. 3217–3228, 2016.

27. Akerboom, J., T.-W. Chen, T. Wardill, L. Tian, J. Marvin, S. Mutlu, N. C. Calderón, F. Esposti, B. Borghuis, X. R. Sun, A. Gordus, M. Orger, R. Portugues, F. Engert, J. J. Macklin, A. Filosa, A. Aggarwal, R. Kerr, R. Takagi, S. Kracun, E. Shigetomi, B. Khakh, H. Baier, L. Lagnado, S. Wang, C. Bargmann, B. E. Kimmel, V. Jayaraman, K. Svoboda, D. S. Kim, E. Schreiter, and L. Looger *Journal of Neuroscience*, Vol. 32, no. 40, pp. 13819–13840, 2012.

28. Zhao, Y., S. Araki, J. Wu, T. Teramoto, Y.-F. Chang, M. Nakano, A. S. Abdelfattah, M. Fujiwara, T. Ishihara, T. Nagai, and R. E. Campbell, "An expanded palette of genetically encoded ca2+ indicators," *Science*, Vol. 333, no. 6051, pp. 1888–1891, 2011.

29. Zariwala, H. A., B. G. Borghuis, T. M. Hoogland, L. Madisen, L. Tian, C. I. De Zeeuw, H. Zeng, L. L. Looger, K. Svoboda, and T.-W. Chen, "A cre-dependent gcamp3 reporter mouse for neuronal imaging in vivo," *Journal of Neuroscience*, Vol. 32, no. 9, pp. 3131–3141, 2012.

30. Cengiz, N., G. Öztürk, E. Erdogan, A. Him, and E. K. Oguz, "Consequences of neurite transection in vitro," *Journal of Neurotrauma*, Vol. 29, no. 15, pp. 2465–2474, 2012.

31. Gross, G. W., B. K. Rhoades, D. L. Reust, and F. U. Schwalm, "Stimulation of monolayer networks in culture through thin-film indium-tin oxide recording electrodes," *Journal of Neuroscience Methods*, Vol. 50, no. 2, pp. 131–143, 1993.

32. Wagenaar, D. A., J. Pine, and S. M. Potter, "Effective parameters for stimulation of dissociated cultures using multi-electrode arrays," *Journal of Neuroscience Methods*, Vol. 138, no. 1, pp. 27–37, 2004.

33. Chisholm, K. I., N. Khovanov, D. M. Lopes, F. La Russa, and S. B. McMahon, "Large scale in vivo recording of sensory neuron activity with gcamp6," *eNeuro*, Vol. 5, no. 1, 2018.

34. Emery, E. C., A. P. Luiz, S. Sikandar, R. Magnúsdóttir, X. Dong, and J. N. Wood, "In vivo characterization of distinct modality-specific subsets of somatosensory neurons using gcamp," *Science Advances*, Vol. 2, no. 11, 2016.

35. Johnstone, A. F., G. W. Gross, D. G. Weiss, O. H.-U. Schroeder, A. Gramowski, and T. J. Shafer, "Microelectrode arrays: A physiologically based neurotoxicity testing platform for the 21st century," *NeuroToxicology*, Vol. 31, no. 4, pp. 331–350, 2010.

36. Schindelin, J., I. Arganda-Carreras, E. Frise, V. Kaynig, M. Longair, T. Pietzsch, S. Preibisch, C. Rueden, S. Saalfeld, B. Schmid, J.-Y. Tinevez, D. J. White, V. Hartenstein, K. Eliceiri, P. Tomancak, and A. Cardona, "Fiji: an open-source platform for biological-image analysis," *Nature Methods*, Vol. 9, no. 7, pp. 676–682, 2012.

37. Harris, K. D., R. Q. Quiroga, J. Freeman, and S. L. Smith, "Improving data quality in neuronal population recordings," *Nature Neuroscience*, Vol. 19, no. 9, pp. 1165–1174, 2016.

38. Jang, M. J., and Y. Nam, "Neuroca: integrated framework for systematic analysis of spatiotemporal neuronal activity patterns from large-scale optical recording data," *Neurophotonics*, Vol. 2, no. 3, 2015.

39. Mormann, F., K. Lehnertz, P. David, and C. E. Elger, "Mean phase coherence as a measure for phase synchronization and its application to the eeg of epilepsy patients," *Physica D: Nonlinear Phenomena*, Vol. 144, no. 3, pp. 358–369, 2000.

40. Fernandez-Montoya, J., C. Avendano, and P. Negredo, "The glutamatergic system in primary somatosensory neurons and its involvement in sensory input-dependent plasticity," *International Journal of Molecular Sciences*, Vol. 19, no. 1, 2018.

41. Brewer, G. J., J. R. Torricelli, E. K. Evege, and P. J. Price, "Optimized survival of hippocampal neurons in b27-supplemented neurobasal, a new serum-free medium combination," *Journal of Neuroscience Research*, Vol. 35, no. 5, pp. 567–576, 1993.

42. Gavazzi, I., R. D. C. Kumar, S. B. McMahon, and J. Cohen, "Growth responses of different subpopulations of adult sensory neurons to neurotrophic factors in vitro," *European Journal of Neuroscience*, Vol. 11, no. 10, pp. 3405–3414, 1999.

43. Tanaka, K., T. Tsukahara, N. Hashimoto, N. Ogata, Y. Yonekawa, T. Kimura, and T. Taniguchi, "Effect of nerve growth factor on delayed neuronal death after cerebral ischaemia," *Acta Neurochirurgica*, Vol. 129, no. 1, pp. 64–71, 1994.

44. Cheng, C.-F., J.-K. Cheng, C.-Y. Chen, R.-H. Rau, Y.-C. Chang, and M.-L. Tsaur, "Nerve growth factor-induced synapse-like structures in contralateral sensory ganglia contribute to chronic mirror-image pain," *PAIN*, Vol. 156, no. 11, 2015.

45. Wainger, B. J., E. D. Buttermore, J. T. Oliveira, C. Mellin, S. Lee, W. A. Saber, A. J. Wang, J. K. Ichida, I. M. Chiu, L. Barrett, E. A. Huebner, C. Bilgin, N. Tsujimoto, C. Brenneis, K. Kapur, L. L. Rubin, K. Eggan, and C. J. Woolf, "Modeling pain in vitro using nociceptor neurons reprogrammed from fibroblasts," *Nature Neuroscience*, Vol. 18, no. 1, pp. 17–24, 2015.

46. Enright, H. A., S. H. Felix, N. O. Fischer, E. V. Mukerjee, D. Soscia, M. Mcnerney, K. Kulp, J. Zhang, G. Page, P. Miller, A. Ghetti, E. K. Wheeler, and S. Pannu, "Long-term non-invasive interrogation of human dorsal root ganglion neuronal cultures on an integrated microfluidic multielectrode array platform," *Analyst*, Vol. 141, pp. 5346–5357, 2016.

47. Lock, J. T., I. Parker, and I. F. Smith, "A comparison of fluorescent ca2+ indicators for imaging local ca2+ signals in cultured cells," *Cell Calcium*, Vol. 58, no. 6, pp. 638–648, 2015.

48. Li, P., A. A. Calejesan, and M. Zhuo, "Atp p2x receptors and sensory synaptic transmission between primary afferent fibers and spinal dorsal horn neurons in rats," *Journal of Neurophysiology*, Vol. 80, no. 6, pp. 3356–3360, 1998.

49. Malet, M., C. Vieytes, K. Lundgren, R. Seal, E. Tomasella, K. Seroogy, T. Hokfelt, G. Gebhart, and P. Brumovsky, "Transcript expression of vesicular glutamate transporters in lumbar dorsal root ganglia and the spinal cord of mice - effects of peripheral axotomy or hindpaw inflammation," *Neuroscience*, Vol. 248, pp. 95–111, 2013.

50. Broussard, G. J., Y. Liang, M. Fridman, E. K. Unger, G. Meng, X. Xiao, N. Ji, L. Petreanu, and L. Tian, "In vivo measurement of afferent activity with axon-specific calcium imaging," *Nature Neuroscience*, Vol. 21, no. 9, pp. 1272–1280, 2018.

51. Gu, Y., Y. Chen, X. Zhang, G.-W. Li, C. Wang, and L.-Y. M. Huang, "Neuronal soma-satellite glial cell interactions in sensory ganglia and the participation of purinergic receptors," *Neuron Glia Biology*, Vol. 6, no. 1, pp. 53–62, 2010.

52. Huang, L.-Y. M., Y. Gu, and Y. Chen, "Communication between neuronal somata and satellite glial cells in sensory ganglia," *Glia*, Vol. 61, no. 10, pp. 1571–1581, 2013.

53. E., P., "The satellite cells of the sensory ganglia," *Adv Anat Embryol Cell Biol.*, Vol. 65, pp. 1–111, 1981.

54. Garriga, J., G. Laumet, S.-R. Chen, Y. Zhang, J. Madzo, J.-P. J. Issa, H.-L. Pan, and J. Jelinek, "Nerve injury-induced chronic pain is associated with persistent dna methylation reprogramming in dorsal root ganglion," *Journal of Neuroscience*, Vol. 38, no. 27, pp. 6090–6101, 2018.

55. Renthal, W., I. Tochitsky, L. Yang, Y. Cheng, E. Li, R. Kawaguchi, D. Geschwind, and C. Woolf, "Transcriptional reprogramming of distinct peripheral sensory neuron subtypes after axonal injury," *Neuron*, Vol. 108, no. 1, pp. 128–144, 2020.

56. MartiÂnez-Lavin, M., "Dorsal root ganglia: fibromyalgia pain factory?," *Clinical Rheumatology*, Vol. 40, no. 2, pp. 783–787, 2021.

57. Esposito, M. F., R. Malayil, M. Hanes, and T. Deer, "Unique characteristics of the dorsal root ganglion as a target for neuromodulation," *Pain Medicine*, Vol. 20, pp. S23–S30, 06 2019.

58. Obien, M. E. J., K. Deligkaris, T. Bullmann, D. J. Bakkum, and U. Frey, "Revealing neuronal function through microelectrode array recordings," *Frontiers in Neuroscience*, Vol. 8, p. 423, 2015.

59. Friedrich, J., W. Yang, D. Soudry, Y. Mu, M. B. Ahrens, R. Yuste, D. S. Peterka, and L. Paninski, "Multi-scale approaches for high-speed imaging and analysis of large neural populations," *PLOS Computational Biology*, Vol. 13, pp. 1–24, 08 2017.

60. Marta, B., P. Alexey, B. Stefano, T. Jacopo, S. Marianna, L. Timothee, C. Ilaria, G. Arseniy, M. Irina, A. Alberto, K. Victor, P. Valentina, and C. Michela, "Closed-loop systems and in vitro neuronal cultures: Overview and applications," *Adv Neurobiol*, Vol. 22, pp. 351–387, 2019.

61. Ju, H., M. R. Dranias, G. Banumurthy, and A. M. VanDongen, "Spatiotemporal memory is an intrinsic property of networks of dissociated cortical neurons," *Journal of Neuroscience*, Vol. 35, no. 9, pp. 4040–4051, 2015.

62. Mosbacher, Y., F. Khoyratee, M. Goldin, S. Kanner, Y. Malakai, M. Silva, F. Grassia, Y. B. Simon, J. Cortes, A. Barzilai, T. Levi, and P. Bonifazi, "Toward neuroprosthetic real-time communication from in silico to biological neuronal network via patterned optogenetic stimulation," *Scientific Reports*, Vol. 10, no. 1, 2020.

63. Tafazoli, S., C. J. MacDowell, Z. Che, K. C. Letai, C. R. Steinhardt, and T. J. Buschman, "Learning to control the brain through adaptive closed-loop patterned stimulation," *Journal of Neural Engineering*, Vol. 17, no. 5, p. 056007, 2020.

64. Wagenaar, D. A., J. Pine, and S. M. Potter, "Searching for plasticity in dissociated cortical cultures on multi-electrode arrays," *Journal of Negative Results in BioMedicine*, Vol. 5, no. 1, 2006.

65. Odawara, A., H. Katoh, N. Matsuda, and I. Suzuki, "Induction of long-term potentiation and depression phenomena in human induced pluripotent stem cell-derived cortical neurons," *Biochemical and Biophysical Research Communications*, Vol. 469, no. 4, pp. 856–862, 2016.

66. Lapp, H., T. Bruegmann, D. Malan, S. Friedrichs, C. Kilgus, A. Heidsieck, and P. Sasse, "Frequency-dependent drug screening using optogenetic stimulation of human ipsc-derived cardiomyocytes," *Scientific Reports*, Vol. 7, no. 1, 2017.

67. Chan, H.-L., M.-A. Lin, T. Wu, S.-T. Lee, Y.-T. Tsai, and P.-K. Chao, "Detection of neuronal spikes using an adaptive threshold based on the max-min spread sorting method," *Journal of Neuroscience Methods*, Vol. 172, no. 1, pp. 112–121, 2008.

68. Caro-Martín, C. R., J. Delgado-García, A. Gruart, and R. Sánchez-Campusano, "Spike sorting based on shape, phase, and distribution features, and k-tops clustering with validity and error indices," *Scientific Reports*, Vol. 8, no. 1, p. 17796, 2018.

69. Mena, G. E., L. E. Grosberg, S. Madugula, P. Hottowy, A. Litke, J. Cunningham, E. J. Chichilnisky, and L. Paninski, "Electrical stimulus artifact cancellation and neural spike detection on large multi-electrode arrays," *PLOS Computational Biology*, Vol. 13, pp. 1–33, 11 2017.

70. Pandarinath, C., E. T. Carlson, and S. Nirenberg, "A system for optically controlling neural circuits with very high spatial and temporal resolution," in *13th IEEE International Conference on BioInformatics and BioEngineering*, pp. 1–6, 2013.

71. Erofeev, A., E. Gerasimov, A. Lavrova, A. Bolshakova, E. Postnikov, I. Bezprozvanny, and O. L. Vlasova, "Light stimulation parameters determine neuron dynamic characteristics," *Applied Sciences*, Vol. 9, no. 18, 2019.

72. Ishizuka, T., M. Kakuda, R. Araki, and H. Yawo, "Kinetic evaluation of photosensitivity in genetically engineered neurons expressing green algae light-gated channels," *Neuroscience Research*, Vol. 54, no. 2, pp. 85–94, 2006.

73. Satuvuori, E., M. Mulansky, N. Bozanic, I. Malvestio, F. Zeldenrust, K. Lenk, and T. Kreuz, "Measures of spike train synchrony for data with multiple time scales," *Journal of Neuroscience Methods*, Vol. 287, pp. 25–38, 2017.

74. Eguia, M. C., G. C. Garcia, and S. A. Romano, "A biophysical model for modulation frequency encoding in the cochlear nucleus," *Journal of Physiology-Paris*, Vol. 104, no. 3, pp. 118–127, 2010. Neural Coding.

75. Lu, Q., T. H. Ganjawala, A. Krstevski, G. W. Abrams, and Z.-H. Pan, "Comparison of aav-mediated optogenetic vision restoration between retinal ganglion cell expression and on bipolar cell targeting," *Molecular Therapy - Methods and Clinical Development*, Vol. 18, pp. 15–23, 2020.

76. Zhang, F., L.-P. Wang, M. Brauner, J. F. Liewald, K. Kay, N. Watzke, P. G. Wood, E. Bamberg, G. Nagel, A. Gottschalk, and K. Deisseroth, "Multimodal fast optical interrogation of neural circuitry," *Nature*, Vol. 446, no. 7136, pp. 633–639, 2007.

77. Steude, A., E. C. Witts, G. B. Miles, and M. C. Gather, "Arrays of microscopic organic leds for high-resolution optogenetics," *Science Advances*, Vol. 2, no. 5, 2016.

78. Barral, J., and A. D. Reyes, "Optogenetic stimulation and recording of primary cultured neurons with spatiotemporal control," *Bio-protocol*, Vol. 7, no. 12, 2017.

79. Muzzi, L., G. Hassink, M. Levers, M. Jansman, M. Frega, J. Hofmeijer, M. van Putten, and J. le Feber, "Mild stimulation improves neuronal survival in an in vitro model of the ischemic penumbra," *Journal of Neural Engineering*, Vol. 17, no. 1, p. 016001, 2019.

80. Pulizzi, R., G. Musumeci, C. V. den Haute, S. V. D. Vijver, V. Baekelandt, and M. Giugliano, "Brief wide-field photostimuli evoke and modulate oscillatory reverberating activity in cortical networks," *Scientific Reports*, Vol. 6, 2016.

81. Hu, C., R. Sam, M. Shan, V. Nastasa, M. Wang, T. Kim, M. Gillette, P. Sengupta, and G. Popescu, "Optical excitation and detection of neuronal activity," *Journal of Biophotonics*, Vol. 12, no. 3, p. e201800269, 2019.

82. Li, W., *Optogenetic control of in vitro neural networks on multi-electrode arrays*. Dissertation, RWTH Aachen University, Aachen, 2017.

83. Schmieder, F., S. D. Klapper, N. Koukourakis, V. Busskamp, and J. Czarske, "Optogenetic stimulation of human neural networks using fast ferroelectric spatial light modulator-based holographic illumination," *Applied Sciences*, Vol. 8, no. 7, 2018.

84. Welkenhuysen, M., L. Hoffman, Z. Luo, A. D. Proft, C. V. den Haute, V. Baekelandt, Z. Debyser, G. Gielen, R. Puers, and D. Braeken, "An integrated multi-electrode-optrode array for in vitro optogenetics," *Scientific Reports*, Vol. 6, 2016.

85. Twyford, P. T., *Spatiotemporally Precise Optical Stimulation System for Controlling Neural Activity In-Vitro*. Dissertation, University of Florida, Florida, 2011.

86. Pimashkin, A., A. Gladkov, I. Mukhina, and V. Kazantsev, "Adaptive enhancement of learning protocol in hippocampal cultured networks grown on multielectrode arrays," *Frontiers in Neural Circuits*, Vol. 7, p. 87, 2013.

87. Newman, J., M. fai Fong, D. Millard, C. Whitmire, G. B. Stanley, and S. M. Potter, "Optogenetic feedback control of neural activity," *eLife*, Vol. 4, 2015.

88. Massobrio, P., J. Tessadori, M. Chiappalone, and M. Ghirardi, "In vitro studies of neuronal networks and synaptic plasticity in invertebrates and in mammals using multielectrode arrays," *Neural Plasticity*, Vol. 2015, 2015.

89. To, W., D. D. Ridder, J. Hart, and S. Vanneste, "Changing brain networks through non-invasive neuromodulation," *Frontiers in Human Neuroscience*, Vol. 12, 2018.

90. Turesson, H., O. Rodríguez-Sierra, and D. Paré, "Intrinsic connections in the anterior part of the bed nucleus of the stria terminalis.," *Journal of neurophysiology*, Vol. 109 10, pp. 2438–50, 2013.

91. Wagenaar, D., R. Madhavan, J. Pine, and S. M. Potter, "Controlling bursting in cortical cultures with closed-loop multi-electrode stimulation," *The Journal of Neuroscience*, Vol. 25, pp. 680 – 688, 2005.

92. Brzosko, Z., W. Schultz, and O. Paulsen, "Retroactive modulation of spike timing-dependent plasticity by dopamine," *eLife*, Vol. 4, 2015.

93. Feldman, D., "The spike-timing dependence of plasticity," *Neuron*, Vol. 75, pp. 556–571, 2012.